

# A Similarity-Based Multiobjective Evolutionary Algorithm for Deployment Optimization of Near Space Communication System

Maoguo Gong, *Senior Member, IEEE*, Zhao Wang, Zexuan Zhu and Licheng Jiao, *Senior Member, IEEE*

**Abstract**—The deployment of the airships plays a key role in maximizing the performance of the near space communication system. The main problem is how to strike a balance between the conflicting network speed and coverage for complex user distribution. In this paper, we propose a multiobjective deployment optimization model considering path loss, user demand and inner structure. Under the framework of the multiobjective evolutionary algorithm based on decomposition (MOEA/D), we propose a similarity-based multiobjective evolutionary algorithm to optimize this problem. The proposed algorithm is motivated by the population’s perception on the decision variable space. The proposed algorithm perceives the decision variable space by deploying airships to latent regions. The perceptions of different solutions are related by the similarity between their deployments and utilized differently by crossover and mutation. The proposed algorithm is tested on five designed problems compared with MOEA/D with the other popular reproduction operators. We also test the proposed scheme integrated with another two popular algorithms. The experimental results show that the similarity-based MOEA/D outperforms the other algorithms significantly in detecting hotspots, tracking multiple hotspots and safely deploying airships for most cases. The proposed scheme also works well with the other algorithms.

**Index Terms**—Near space communication system, deployment optimization, multiobjective optimization, evolutionary algorithm

## I. INTRODUCTION

THE near space is about 20 to 100 kilometers high above sea level, encompassing stratosphere, mesosphere and thermosphere [1]. At this altitude, there are fewer aircrafts, which makes it safe for the airships in the near space. The temperature is between -90 degrees Celsius and 30 degrees Celsius, which is suitable for most devices. For 99% of the time, the wind speed is smaller than 70 knots at 80000ft, which makes it easier for airships to maneuver. The solar energy density in the near space is much higher than that on the ground, while the cosmic radiation is weaker than that in orbit

Maoguo Gong, Zhao Wang and Licheng Jiao are with Key Laboratory of Intelligent Perception and Image Understanding of Ministry of Education, International Research Center for Intelligent Perception and Computation, Xidian University, No.2 South TaiBai Road, Xian 710071, China. E-mail: gong@ieee.org.

Zexuan Zhu is with the College of Computer Science and Software Engineering, Shenzhen University, China.

This work was supported by the National Natural Science Foundation of China (Grant nos. 61273317, 61422209 and 61471246), the National Top Youth Talents Program of China, the Specialized Research Fund for the Doctoral Program of Higher Education (Grant no. 20130203110011) and the Fundamental Research Fund for the Central Universities (Grant no. K5051202053).

space [2]. Thus the environment of the near space is desirable for airships.

The near space communication system (NSCS) is a burgeoning alternative solution to the growing demand for communication of the modern world. At present, there are two main wireless communication systems: the terrestrial wireless communication system (TWCS) and the satellite communication system (SCS). A comparison of these three communication systems is shown in Table I.

The near space platforms are widely used in synthetic aperture radar due to its high resolution and wide swath [3], [4]. They are also used in earth observation because of convenient deployment and low cost [5]. NSCS is drawing increasing interest due to its advantages over TWCS and SCS [6], [7]. For example, Google has been running an NSCS project, namely, Google Balloon in New Zealand, Brazil, and the United States since 2013. This project has succeeded in providing internet connection for the ground users.

The airship deployment is crucial to the performance of NSCS. Due to the limited airship resource, NSCS is unable to provide high speed network while maintaining a large coverage. Optimal tradeoff solutions is required for the managers of NSCS to choose from for different scenarios. Thus the problem is a multiobjective optimization problem. There has been some researches on the deployment optimization of NSCS concerning network speed [8], energy consumption [9], ground target overlaying and detection quality [10]. The deployment optimization is also solved as a multiobjective optimization problem [11].

For the deployment optimization of NSCS, there are no literatures considering path loss, routing efficiency, user demand and safety issue at the same time, which are the main concerns of the modern communication system. All the works so far just consider some of the above four aspects. In this paper, the proposed NSCS model is the first to consider the four major aspects above and provides a general model for the deployment optimization of NSCS. This model can be easily extended with more details of modern communication systems. The deployment pattern, which is common in many other deployment optimization problems, is also studied for the first time. A similarity-based multiobjective evolutionary algorithm is also proposed to optimize the deployment of NSCS. This algorithm is motivated by the relations of the deployments of different solutions. A deployment solution implicitly divides the whole area into several latent regions by deploying airships to the best available positions: one airship in a latent region.

TABLE I  
THE COMPARISON OF NSCS, TWCS AND SCS

	NSCS	TWCS	SCS
Network speed	<b>High</b>	<b>High</b>	Low
Coverage	<b>Global</b>	Unable to cover remote area	<b>Global</b>
Price	<b>Low</b>	<b>Low</b>	High for daily use
Large-scale civil use	Yes	Yes	No
Robustness	<b>Disaster-independent</b>	Fragile	<b>Disaster-independent</b>
Deployment cost	<b>Low</b>	Expensive in remote area	High
Deployment complexity	Airships can be released almost anywhere	limited by many factors: terrain, health concern, etc.	Difficult
Environment safety	Safe, no uncontrollable debris	Safe	Threatened by space debris

Thus the deployment of an individual is actually its perception of this area from the perspective of evolutionary algorithm. For multiobjective evolutionary algorithm based on decomposition (MOEA/D), different subproblems treat the whole area differently. Neighbor subproblems have similar perceptions. For two individuals, the perceptions can be combined to form a common perception of the whole area by classifying airships of each individual into common latent regions based on the similarity between them. On one hand, the common perception of the two individuals helps redistribute airships among latent regions. On the other hand, the position differences of the airships inside a latent region provide promising direction for searching optimal positions in this region. The proposed algorithm is tested on the five test problems and the experimental results show that the similarity-based MOEA/D performs well in detecting the hotspots, tracking multiple hotspots and safely deploying airships. The experimental results also show that the similarity-based reproduction scheme can be easily integrated with the other algorithms and works well.

This paper has two main contributions:

- From the perspective of NSCS, a general model is proposed which encompasses the important aspects of NSCS. For NSCS, the communication fading is calculated using a general model, and the routing efficiency is calculated as well. We detail the user demand so that NSCS will treat areas of various types differently. A safety issue is also considered. These four aspects cover the major concerns of modern communication systems from three facets: NSCS, the communication process and users. To our best knowledge, this is the first general NSCS model considering these four aspects.
- From the algorithmic perspective, a similarity-based MOEA/D with shift initialization is proposed to optimize the deployment of NSCS. The proposed algorithm is the first to utilize the population perception. Based on the population perception, the similarity-based MOEA/D is effective in optimizing the deployment of NSCS.

The rest of this paper is organized as follows. In Section II, we first summarize some recent researches on the deployment problems of NSCS and other similar network systems. The difficulties are described as well. The detailed NSCS model is described in Section III. In Section IV, we introduce the population's perceptions and propose the similarity-based

MOEA/D. In Section V, the designed test problems are described and the similarity-based MOEA/D is tested on these problems. The experimental results is discussed as well. In Section VI, we conclude this paper and present the future work.

## II. BACKGROUND

The deployment optimization of NSCS is similar to those of some other fields like: sensor network, cellular network and smart grid. In this section, we will review some researches in these domains and investigate the relations and differences of the deployment optimization problems between these domains and NSCS.

To deploy sensors that are not easy to access, static deployment approaches are applied. In [12], a forest fire probability model is obtained and the deployment problem is transformed to a  $k$ -coverage maximization problem. The authors propose a distributed algorithm to obtain a multi-degree sensor deployment. In [13], a fast chromosome decoding scheme is integrated with the Genetic Algorithm to obtain the optimal deployment. For sensors with mobility, the authors in [14] minimize the energy consumption while maximizing the coverage using Voronoi Diagram. Compared with sensor deployment, the deployment of NSCS can be considered as locally static and dynamic problem.

The objectives of sensor deployment optimization are different for various applications. One of the most important objectives is coverage [15]. Luo *et al.* [16] propose a weighted grid deployment optimization to maximize mobile sensor coverage. In [17], the authors study the optimal pattern of optimal coverage and connectivity, which is instructive in searching deployment solutions. One important application is barrier coverage in intrusion detection. He *et al.* [18] present a situation where the line-based deployment is a local optimum and a deterministic deployment algorithm is proposed to generate a curved-based deployment. In addition to 2-D coverage, Temel *et al.* [19] optimize coverage a 3-D terrain coverage. The novelty of this paper is that a Cat Swarm Optimization algorithm is combined with a wavelet transform to optimize the sensor deployment. For the deployment of smart grid and cellular network, the transmission process is considered while maximizing the coverage. In [20], the authors extend the channel model with smart meters and solve

the combined objective to obtain a reliable networks. Cui *et al.* [21] investigate how to deploy the base stations so that the communication demand of smart grid is met. For a wireless communication system, the coverage and quality of communication are two significant objectives. In [22], a two stage framework is proposed to optimize the coverage and the averaged received power. The simulated annealing algorithm is used to optimize the coverage and system capacity at the same time in [23]. For NSCS, on one hand, the system should try to cover as large area as possible. On the other hand, high speed network is required. As a result, the deployment optimization of NSCS is a multiobjective optimization problem.

There are many algorithms developed for the deployment optimization of sensor network, smart grid and cellular network. The virtual force based algorithm introduces a virtual force that reflects the relations among adjacent nodes [24]. Computational geometry based algorithms decide whether a node in a network should be redeployed and where to deploy according to the topology structure [25]. Fuzzy based algorithms are able to handle uncertainty factors in the deployment process and obtain smoother result than the other algorithms do [26]. There are many other algorithms like pattern based, grid based and metaheuristic based algorithms. Due to the complexity and difficulty in solving deployment optimization problems in the real world, the metaheuristic based algorithms, especially evolutionary algorithms, are becoming more popular in these years. Compared with the other deployment optimization methods, the evolutionary algorithms are suitable for solving complex problems, able to provide optimal or near optimal solutions, easy to use and good at handling constraints. In [27], a distributed coevolutionary algorithm is proposed to optimize coverage. The novelty of this paper is that the fitness function combines the neighborhood information of each node, which maximizes the utilization of region information. Some other methods are combined with the evolutionary algorithms to boost the deployment process. Sahin *et al.* [28] optimize the objective functions introduced from virtual force method using a genetic algorithms for a real-time deployment system. In [29], the coverage and lifetime of a sensor network are optimized using a multiobjective genetic algorithm. Jiang *et al.* [27] integrate local information of the deployment with the distributed evolutionary algorithm to optimize the coverage of sensor network.

There are many works for optimizing the deployment of NSCS based on evolutionary algorithms. X. Wang *et al.* [8] combine the communication delay and information entropy as the objective function, and propose a modified genetic algorithm to optimize the deployment. In [9], the simulated annealing algorithm is applied to minimize the energy consumption while maintaining coverage. The authors also proved the solutions' optimality, and the experiment results show that the simulated annealing algorithm can achieve the optimal solution. Yin *et al.* [10] combine four objectives: coverage, ground overlaying, ground target resolution and detection ability into the objective function and propose a adaptive genetic algorithm to optimize the deployment. The novelty of this paper lies on the adaptive crossover and mutation probability which prevent the algorithm from falling into local

optima. In our last paper [11], we first propose a multiobjective optimization problem for NSCS, and optimize the coverage and network speed as a multiobjective optimization problem using MOEA/D.

There are three main difficulties in the deployment optimization of NSCS. First, the deployment of NSCS considers two objectives: coverage and network speed. The network speed is not only affected by the transmission fading between airships and users, but also affected by the routing efficiency inside the airship network. NSCS should maintain a network topology of high routing efficiency while optimizing the coverage and network speed. Second, there are more than one hotspots in an area. Two solutions, which have similar or even the same objective values, may have totally different airship deployment. In another word, there are many positions in a complex area that are suitable for a specific airship. This kind of individual difference will mislead the search process. This is also why we develop a similarity-based reproduction scheme to relate the deployments of different individuals. Third, some optimal positions are not feasible for both two airships due to safety matter. One optimal position is not available for another airship when an airship has already been deployed there. The other airship has to search the neighborhood of the optimal area, which makes it easier to violate the safety constraint.

The problem complexity of deployment optimization of NSCS is NP-hard. We can reduce this problem to a Euclidean  $k$ -center cost problem by removing the constraint, routing efficiency and path loss using the method of restriction. The  $k$ -center cost problem is to deploy  $k$  discs to minimize the total distance from the demand points to the nearest disc center. The Euclidean  $k$ -center cost problem has proven to be an NP-hard problem [30], [31].

Compared with our last work, the major progress of this paper is:

- The network speed is more precise. In our last paper, the speed is simply measured by the distance from the users to the nearest airship. In this paper, the network speed is calculated according to a general fading model, and the routing efficiency inside the airship network is also considered.
- The coverage is more accurate. The last paper treats the connect status of the users as the coverage measurement, while the approximate covered area is calculated in this paper.
- In this paper, a safety constraint is included in the model.
- In this paper, we deeply investigate the deployment pattern and utilize the relations between deployments of different individuals in the evolutionary process. Based on these relations, a shift initialization and a general similarity-based reproduction scheme are proposed which can be easily integrated with the other algorithms.

### III. THE MODELING OF DEPLOYMENT OPTIMIZATION PROBLEM

The NSCS model in this paper considering the aspects below:

- The path loss [32] and the routing efficiency of inner structure which affect the network speed [33].

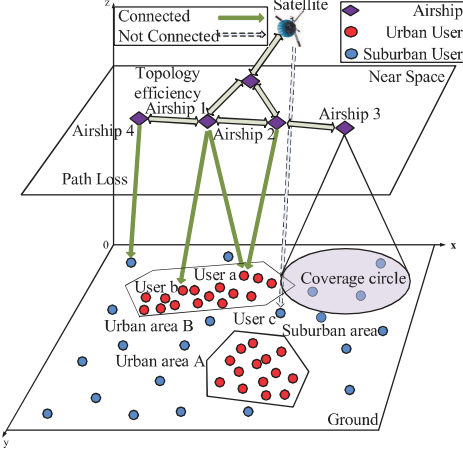


Fig. 1. The Near Space Communication System Model

- Distributed wireless communication technique in communication between users and airships [34].
- Two user types with different communication demands: the urban user and the suburban user.
- The maximum communication distance and safety distance between airships.

The proposed NSCS model is shown in Fig. 1. Two objectives are optimized. The first objective is network speed, which is relevant to the path loss between NSCS and the users and is also affected by the routing efficiency. The path loss and routing efficiency are integrated together to calculated a final network speed provided for the users. The satellite provides the network connection if the users cannot connect to the airships. The second objective is the coverage. The coverage is calculated without counting overlap. For users on the ground, users in different areas have different network speed demand, and redundant network speed is wasted if the demand of a certain user is fulfilled.

Different areas weigh the two objectives differently. On one hand, the dense urban users require high network speed. Thus NSCS should gather the airships around urban area. On the other hand, NSCS should also cover as large area as possible, which requires a spread of the airships. Limited airships have these two objectives conflicts with each other. Thus NSCS should strike a balance between the network speed and coverage and provide a set of Pareto optimal solutions for decision makers to deal with different scenarios. The problem is naturally a multiobjective optimization problem. The decision variables to be optimized are the positions of  $M$  airships:  $\{(x_1, y_1), \dots, (x_M, y_M)\}$ . To improve the performance, NSCS works with one satellite to provide network connection. In this paper, we assume that all the airships have the same altitude.

#### A. The first objective: Network speed

The network speed can be measured by the network capacity. A user gets higher network speed by obtaining more capacity related resources like bigger bandwidth, permission to connect to the base station, more processing capability etc. The

capacity obtained by a user is affected by many factors. In this paper, we consider the three main factors: path loss, routing efficiency and distributed wireless communication technique. The network capacity are described below.

*1) user model:* The users determine the deployment of modern communication systems. Not only the user distribution but also the user demand will affect the performance of modern communication systems. The deployment optimization algorithms are required to deal with different user distributions and fulfill different user demands. The deployment also should be optimized to avoid capacity waste.

In Fig. 1, there are two types of users: the urban users and the suburban users. Dense urban users are located in: urban area A and B. The users of different types have different demands for communication. The urban users' maximum demand is denoted as  $DE_{ub}$ , and the suburban users' maximum demand is denoted with  $DE_{sub}$ . In general, the urban users require more network capacity to gain higher network speed than the suburban users do, i.e.:

$$DE_{ub} > DE_{sub} \quad (1)$$

However, the other user demand relations can be applied here. Every user tries to connect to the airships that cover it like user  $a$  and user  $b$  as shown in Fig. 1. If a user, like user  $c$ , is not covered by NSCS, it connects to the satellite instead.

*2) path loss:* For modern communication system, the path loss affects the communication quality. Thus it is inevitable when optimizing the deployment. Small path loss provides communication of high quality and saves resource. Thus the path loss makes NSCS consider not only the urban users but also the suburban users.

The path loss is related to many factors: multi-path propagation [35], diffraction, ground reflection, scattering [36], shadowing/blocking [37] etc. Due to the complexity of communication environment, there exists many models simulating the path loss: Nakagami fading, Rician fading, Rayleigh fading etc [37]. A typical and common path loss model is provided by the Friis equation [38], [39]:

$$P_r = P_t G_t G_r \left( \frac{\lambda_c}{4\pi x} \right)^2 \quad (2)$$

where  $P_r$  is the received signal power which is directly related with the network capacity obtained by the users.  $P_t$  is the signal transmission power.  $\lambda_c$  is the wavelength.  $G_t$  and  $G_r$  are the transmission and receiving gain of antenna respectively and  $x$  is the transmission distance. Many fading models are derived from the Friis equation. Following the Friis equation, it can be noticed that the received power is positively related with the transmission power and negatively related with the transmission distance. The higher the  $P_r$ , the more stable and faster the network will be. To avoid unnecessary complexity,  $P_r$  is generalized as the network capacity.

For general purpose, the actual capacity ratio  $RU_{jl}$  obtained by user  $l$  in position  $(x_l, y_l, z_l)$  from an airship  $j$  in position  $(x_j, y_j, z_j)$  is defined as follows:

$$RU_{jl} = 1 - E_f(D_{jl})^3 \quad (3)$$

$$D_{jl} = \sqrt{(x_j - x_l)^2 + (y_j - y_l)^2 + (z_j - z_l)^2} \quad (4)$$

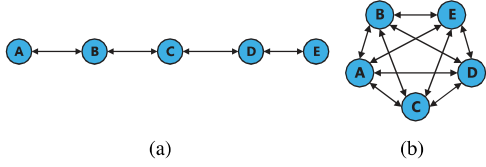


Fig. 2. The routing efficiency model. (a). deployment of low routing efficiency. (b). deployment of high routing efficiency

where  $RU_{jl} \in [0, 1]$ , and  $E_f$  is the fading factor. Other fading models can be applied here.

The actual capacity  $CU_{jl}$  that user  $l$  gains from airship  $j$  is:

$$CU_{jl} = CE_j RU_{jl} \quad (5)$$

where  $CE_j$  is the actual capacity that airship  $j$  assigns to user  $l$ .

3) *routing efficiency*: For a large-scale NSCS, the routing efficiency is directly related with the message delivery efficiency inside NSCS. An NSCS with efficient routing can deliver message by fewer airships and consume less processing time. This requires algorithms to maintain good network structure when searching for the optimal solutions.

If two airships cannot communicate with each other directly, then the signal should be relayed by other airships. There has been many researches on the routing efficiency [40]–[42], according to which, the routing efficiency is mainly affected by two factors: the number of nodes of the route and the path loss. Two examples of different routing efficiencies are shown in Fig. 2. On average, the message packets travel a longer distance in Fig. 2 (a) than they do in Fig. 2 (b). Therefore the routing efficiency of one airship can be measured by the total distance from it to all the other airships. For  $M$  airships, we assume they have the same original capacity. The original capacity of airship  $j$  is  $CT_j$ . Due to the routing efficiency, the remaining capacity  $CA_j$  of airship  $j$  is:

$$DT_j = \sum_{i=1, i \neq j}^M D_{ji}^{route} \quad (6)$$

$$RE_j = 1 - E_r(DT_j)^3 \quad (7)$$

$$CA_j = CT_j RE_j \quad (8)$$

$$D_{ji}^{route} = D_{j_1 j_{r_1}} + D_{j_{r_N} j_2} + \sum_{i=1}^{N-1} D_{j_{r_i} j_{r_{i+1}}} \quad (9)$$

where  $DT_j$  is the summation of the distances of the shortest routes from airship  $j$  to all the other airships.  $RE_j$  is the ratio of the remaining capacity to the original capacity of airship  $j$  and  $RE_j \in [0, 1]$ .  $E_r$  is the fading factor of the communication between airships.  $D_{ji}^{route}$  is the length of the shortest communication route, namely,  $(j_1, j_{r_1}, \dots, j_{r_N}, j_2)$  from  $j_1$  to  $j_2$  that contains  $N$  relays.

The remaining capacity  $CA_j$  of airship  $j$  is split equally by all the users that connect to it. With the distributed wireless communication technique, each user can get higher speed by connecting to all the airships that cover it [34]. Assume we

have  $L$  users on the ground, the capacity  $CE_j$  assigned to each user connecting to airship  $j$  is:

$$CE_j = \frac{CA_j}{\sum_{l=1}^L S_{jl}} \quad (10)$$

where  $S_{jl}$  is the connection indicator:

$$S_{jl} = \begin{cases} 1, & \text{if user } l \text{ connects to airship } j \\ 0, & \text{otherwise} \end{cases} \quad (11)$$

For the users that cannot connect to any airships, the satellite provides alternative connection. The satellite capacity  $CS$  is split equally by the users that connect to it. The capacity  $CU_{sl}$  obtained by user  $l$  that connects to the satellite is:

$$CU_{sl} = \frac{CS}{LS} \quad (12)$$

where  $LS$  is the number of users that connect to the satellite. Other routing efficiency models can be applied here as well.

Because of the limited demand of users, superfluous capacity is wasted. Thus the total capacity  $CTU_l$  consumed by urban user  $l$  is:

$$CTU_l = \sum_{j=1}^M CU_{jl} S_{jl} + CU_{sl} \quad (13)$$

if  $\sum_{j=1}^M CU_{jl} S_{jl} + CU_{sl} \leq DE_{ub}$ .

$$CTU_l = DE_{ub} \quad (14)$$

if  $\sum_{j=1}^M CU_{jl} S_{jl} + CU_{sl} > DE_{ub}$ .

The total capacity  $CTU_k$  consumed by suburban user  $k$  is:

$$CTU_k = \sum_{j=1}^M CU_{jk} S_{jk} + CU_{sk} \quad (15)$$

if  $\sum_{j=1}^M CU_{jk} S_{jk} + CU_{sk} \leq DE_{sub}$ .

$$CTU_k = DE_{sub} \quad (16)$$

if  $\sum_{j=1}^M CU_{jk} S_{jk} + CU_{sk} > DE_{sub}$ .

The maximum demand for communication implies that it should avoid capacity surplus when deploying airships around the urban area. The first objective is to maximize the total capacity  $C$  actually consumed by all the users:

$$C = \sum_{l=1}^L CTU_l \quad (17)$$

### B. The second objective: Coverage

To achieve a global coverage, NSCS should cover as large area as possible. We assume that each airship covers a circular area as shown in Fig. 1. The total covered area  $S$  of NSCS with  $M$  airships serves as the second objective:

$$SA_j = \pi r_c^2 \quad (18)$$

$$S = \bigcup_{j=1}^M SA_j \quad (19)$$

where  $r_c$  is the radius of the coverage circle, and  $SA_j$  is the circle area covered by airship  $j$ .

### C. Constraints

It is especially important to maintain a safety distance between any two airships for NSCS. The probability that two airships may crash is high when they get too close to each other. Thus it is necessary to consider safety distance when deploying airships. With this constraint, the optimal positions are available for only one airship, and the algorithms should search around the optimal positions to deploy the other airships.

For any two airships, the maximum communication range is defined as  $D_c$ . To achieve a global coverage, every two airships should be able to communicate with each other directly or through the other relay airships. The routing distance between any two disconnected airships can be considered as infinite. At the meantime, any two airships should keep a safety distance  $D_s$  to avoid collision. Given two airships  $j_1$ :  $(x_{j_1}, y_{j_1})$  and  $j_2$ :  $(x_{j_2}, y_{j_2})$ , constraints are as follows:

$$D_{j_1 j_2} \geq D_s \quad (20)$$

$$D_{j_1 j_2}^{route} < \infty \quad (21)$$

$$D_{j_1 j_2} = \sqrt{(x_{j_1} - x_{j_2})^2 + (y_{j_1} - y_{j_2})^2} \quad (22)$$

where  $D_{j_1 j_2}$  is the distance between  $j_1$  and  $j_2$ .

Based on the analysis above, the deployment optimization of NSCS is formulated as a multiobjective optimization problem:

$$\left\{ \begin{array}{l} \text{maximize } C \\ \text{maximize } S \\ \text{subject to (20) and (21)} \end{array} \right. \quad (23)$$

## IV. DEPLOYMENT OPTIMIZATION WITH SIMILARITY-BASED MOEA/D

MOEA/D is a popular algorithm of high efficiency for solving multiobjective optimization problem [43]–[46]. The subproblems instinctively maintain population diversity [47]–[49] and group the individuals that have similar perceptions on the variable space. For the deployment optimization of NSCS, the algorithms perceive the variable space by deploying airships to different regions. Due to different weight vectors, the neighbor individuals have similar but not the same perceptions on the variable space. The similarity and difference of these perceptions provide important information for adjusting deployment among and inside these regions, which is implemented by the reproduction operators. In this section, we propose a similarity-based MOEA/D which utilizes the perception information.

### A. Shift initialization

The initialization is important to the performance of the evolutionary algorithms. The uniformly distributed initial population can not track the user distribution, in other words, the uniformly distributed population cannot reflect the distribution of the Pareto optimal solutions. Thus we should initialize the population utilizing the user distribution so that the initial population can be as close to the distribution of the Pareto optimal solutions as possible.

---

### Algorithm 1 Similarity-based MOEA/D

---

```

1: Input
    • the size of neighborhood: H
    • the parameters of NSCS
    • the other parameters of the similarity-based MOEA/D
2: Initialization:
    • Generate initial population of size  $N$  using shift
      initialization
    • Calculate the objective value and the decomposed
      objective value of each individual
    • Generate  $N$  weight vectors and assign the individuals
      to the subproblems according to the first objective
    • Initialize the external population (EP) as an empty set
3: while termination criterion is not satisfied do
4:   for  $i=1$  to  $N$  do
5:     Crossover: For subproblem  $i$ , select two subproblems
        $i_a$  and  $i_b$  from its neighbors, and perform crossover
       as described in Section IV-B2. Obtain two offsprings
        $i_{a'}$  and  $i_{b'}$ .
6:     Mutation: For  $i_{a'}$  and  $i_{b'}$ , perform mutation de-
       scribed in Section IV-B3 and obtain two offsprings
        $i_{a''}$  and  $i_{b''}$ .
7:     Repair: For  $i_{a''}$  and  $i_{b''}$ , perform repair operation as
       described in Section IV-B3. Calculate the objective
       value of the two offsprings.
8:     Update:
9:     for  $h = 1$  to  $H$  do
10:      Calculate the decomposed objective value  $f_d(i_{a''} \mid$ 
        $w_h)$  and  $f_d(i_{b''} \mid w_h)$ 
11:      if  $f_d(i_{a''} \mid w_h)$  (or  $f_d(i_{b''} \mid w_h)$ )  $< f_d(i_h \mid w_h)$ 
       then
12:        Replace individual  $i_h$  with  $i_{a''}$  (or  $i_{b''}$ )
13:      end if
14:    end for
15:    Update EP: Remove any individuals dominated by
        $i_{a''}$  or  $i_{b''}$  from EP, and if any of  $i_{a''}$  or  $i_{b''}$  is not
       dominated by any individual in EP, add it to EP
16:  end for
17: end while
18: Output: EP

```

---

It is noted that the first objective has a positive correlation with the number of airships gathering around the hotspots. Therefore we can use the density of the users to guide the initialization. With the airships shifting from the urban areas to the suburban areas, the gathering airships spread out gradually. Thus the capacity of NSCS is less utilized but a larger area is covered, and the generated individuals' concentration shifts from network speed to coverage. Then the objective space is supposed to be covered as uniformly as possible.

The initialization is illustrated in Fig. 3 (a). First, the area is divided into  $P$  blocks:  $\{B_1, \dots, B_i, \dots, B_P\}$ , and the coordinates of the center of each block  $(x_i^B, y_i^B)$  are recorded. The number of users  $U_i, i = 1 \dots P$ , of each block is calculated as well. The block size, i.e.,  $X^B$  in  $x$ -dimension and  $Y^B$  in  $y$ -dimension, should be moderate so that the blocks

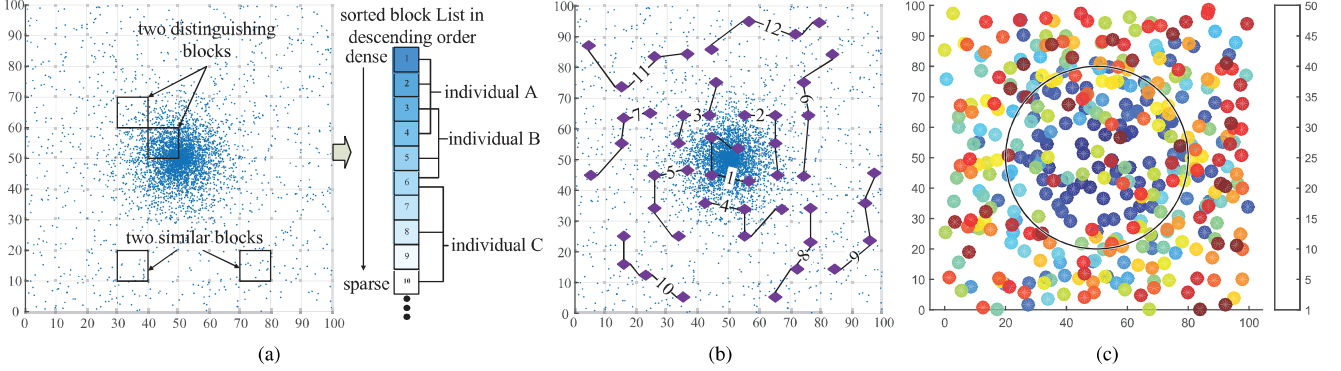


Fig. 3. The shift initialization on single hotspot. (a) The procedure of the shift initialization. (b) An illustration of the distribution of the generated individual with 4 airships. The sequence of each individual is labeled. (c) A simulation of the shift initialization with 4 airships. The airships of 50 individuals are plotted. The color ranges from blue to red as the individuals being generated from the beginning to the end, for example, the airships denoted by blue belong to the first generated individual and those denoted by red are the airships of the last generated individual.

are as distinguished from each other as possible in terms of the number of users. Second, the blocks are sorted in descending order according to the number of users. Third, each new individual tries to select the top blocks that are not selected by the previous individuals to deploy its airships, and the later deployed airships should not conflict with the previously deployed ones according to (20). For individual  $k$ , the airship  $j : (x_{kj}^A, y_{kj}^A), j = 1, \dots, M$  is deployed at:

$$\begin{cases} x_{kj}^A = x_i^B + X^B(\alpha - 0.5) \\ y_{kj}^A = y_i^B + Y^B(\beta - 0.5) \end{cases} \quad (24)$$

where  $\alpha, \beta \sim U(0, 1)$ . If the center position of block  $i$  conflicts with the previously deployed airships according to (20), the initialization will move to the next unselected block to deploy airship  $j$ . After all  $M$  airships of individual  $k$  are deployed, repair operation is performed to adjust the deployment so that (20) and (21) are satisfied. At last, the blocks that are selected by individual  $k$  is labeled. For smooth transition between subproblems, each new individual directly copies several airships from the last individual just like individuals B and C shown in Fig. 3 (a).

The initialization process is terminated when the deployment reaches the boundary or runs out blocks. An illustration of the initial population is shown in Fig. 3 (b), and a simulation is shown in Fig. 3 (c). From Fig. 3 (c), we can notice the shift process of the airships from the urban area to the suburban area with the proceeding of the initialization, which is consistent with the expected process as shown in Fig. 3 (b).

After generating the initial population, all individuals will be sorted in descending order according to the first objective. The weight vectors of the subproblems are generated uniformly and sorted in descending order according to the weight of the first objective. Each individual is assigned to the subproblem with the same order.

The advantages of the shift initialization are:

- All the airships of the entire population are not uniformly distributed but related to user distribution.
- It provides similarity-based MOEA/D an initial population of clear perceptions' structure.
- The initial population is fully utilized.

### B. Similarity-based reproduction operator

*1) motivation:* The reproduction operators play a key role in the performance of MOEA/D. For the deployment optimization of NSCS, each individual perceives the variable space by deploying airships to latent regions where the airships are utilized the most from the objective functions' perspectives. In other words, the deployment of airships is actually the individual's perception of the decision variable space. The perception of an individual forms the latent regions of interest like region  $A$ ,  $B$ ,  $C$  and  $D$  as shown in Fig. 4 (a). For two subproblems that are not neighbors, the perceptions of the individuals on variable space may be different like individual  $a$  and  $c$  in Fig. 4 (a). For neighbor subproblems, the perceptions of the individuals may be similar like individual  $a$  and  $b$ . There also may be more than one latent regions having the similar effect on the objective functions like regions  $C$  and  $E$  of individual  $b$ . The similarity and the difference of the individuals' perceptions are two aspects of heuristic information for MOEA/D to generate new individuals.

Thus the reproduction process comes down to two operations. The first one is how to distribute airships between latent regions. The second one is where to deploy the airships inside latent regions. These two operations are performed by crossover and mutation respectively.

*2) crossover:* The aim of crossover is to distribute airships among latent regions. For example, in Fig. 4 (a), assume we have two individuals  $a$  and  $b$  before performing crossover. The airship 2 of individual  $b$  can be redeployed to region  $A$  to try to improve the performance of NSCS. Based on the perceptions of individual  $a$  and  $b$ , individual  $a$  provides a promising location, where airship 1 is deployed, for individual  $b$  to deploy airship 2. To obtain two individuals' perceptions of a latent region, we need to find out the airships deployed to the same region by each individual.

For two selected individuals  $P : (x_1^P, y_1^P, \dots, x_M^P, y_M^P)$  and  $Q : (x_1^Q, y_1^Q, \dots, x_M^Q, y_M^Q)$ , we use the similarity between the two individuals to evaluate their perceptions. The Euclidean

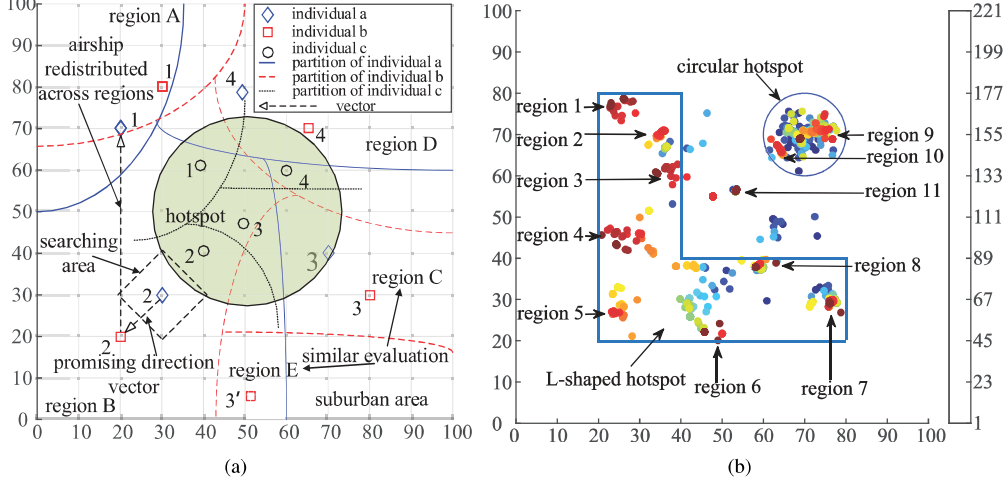


Fig. 4. The reproduction operations of the similarity-based MOEA/D (a). Schematic diagram of three individuals. The area has one circular hotspot with center at  $(50, 50)$  and radius of 20. The subproblems of individual a and b are neighbors, and the subproblem of individual c is not neighbor of either of them. (b). A simulation of 221 individuals in the area with one L-shaped hotspot and one circular hotspot. Each individual has 8 airships. The more similar the colors are, the more closely the corresponding subproblems are related. The latent regions of neighboring individual around 210 are pointed out by arrows.

distance between individuals  $P$  and  $Q$  is:

$$DS(P, Q | Per_0) = \sum_{j=1}^M \sqrt{(x_j^P - x_j^Q)^2 + (y_j^P - y_j^Q)^2} \quad (25)$$

where  $Per_i$  is a permutation of the airships' indexes of individual  $Q$ .  $T$  is the set of all the permutations of set  $\{1, \dots, M\}$ . For individual  $Q$ , the initial permutation of the airships' indexes is denoted as  $Per_0 = (1, \dots, M)$ , and we have:

$$\begin{cases} Per_i = (j_{i1}, \dots, j_{iM}), i = 0, \dots, M! - 1 \\ T = \{Per_0, \dots, Per_{M!-1}\} \\ \{j_{i1}, \dots, j_{iM}\} = \{1, \dots, M\}, i = 0, \dots, M! - 1 \end{cases} \quad (26)$$

The similarity  $SL(P, Q)$  between  $P$  and  $Q$  is defined as the smallest  $DS(P, Q)$  by adjusting the airship sequence of  $Q$ :

$$SL(P, Q | Per_{i_0}) = \min\{DS(P, Q | Per_i) | Per_i \in T\} \quad (27)$$

$$Per_{i_0} = (j_{i_01}, \dots, j_{i_0M}), i_0 \in \{0, \dots, M! - 1\} \quad (28)$$

For airship  $k$  of individual  $P$ , the airship  $j_{i_0k}$  of individual  $Q$  is in the same latent region.

After obtaining the common perception of the two individuals, the airship  $k$  of offspring  $P'$  is deployed as:

$$\begin{cases} (x_k^{P'}, y_k^{P'}) = (x_k^P, y_k^P), \text{ if } \alpha \leq PB_c \\ (x_k^{P'}, y_k^{P'}) = (x_l^Q, y_l^Q), \text{ otherwise} \end{cases} \quad (29)$$

where  $l \neq j_{i_0k}$ , and  $l$  is randomly chosen from  $\{1, \dots, M\}$ .  $PB_c$  is the probability of crossover.

The second offspring  $Q'$  is generated in the same way with the airship sequence of  $P$  being rearranged according to  $Per_{i_0}$ .

3) mutation: The aim of mutation is to search the latent region to find the best position where the airships can be fully utilized. In Fig. 4 (a), assume the crossover has been proceeded, and airship 2 of individual b provides a promising direction vector in region B. According to this direction vector, individual a may improve one objective without deteriorating

the other one too much by searching the area around it. Given two individuals  $P'$  and  $Q'$  generated by crossover, the airship sequence of  $Q'$  is rearranged to obtain the common perception of each latent region and find the airship sequence which satisfies:

$$SL(P', Q' | Per_{i_0}) = \min\{DS(P', Q' | Per_i) | Per_i \in T\} \quad (30)$$

$$Per_{i_0} = (j_{i_01}, \dots, j_{i_0M}) \quad (31)$$

To obtain the promising searching area, the set  $V = \{(x_1^D, y_1^D), \dots, (x_M^D, y_M^D)\}$  of difference vectors and the set  $V' = \{(x_1^{D'}, y_1^{D'}), \dots, (x_M^{D'}, y_M^{D'})\}$  of vertical difference vectors are calculated as:

$$\begin{cases} x_k^D = 0.5(x_k^{P'} - x_{j_{i_0k}}^{Q'}) \\ y_k^D = 0.5(y_k^{P'} - y_{j_{i_0k}}^{Q'}) \\ x_k^{D'} = y_k^D \\ y_k^{D'} = -x_k^D \\ k = 1, \dots, M \end{cases} \quad (32)$$

The airship  $k$  of offspring  $P''$  is generated as:

$$\begin{cases} x_k^{P''} = x_k^{P'} + x_k^D(\alpha - 0.5) + x_k^{D'}(\gamma - 0.5) \\ y_k^{P''} = y_k^{P'} + y_k^D(\beta - 0.5) + y_k^{D'}(\delta - 0.5) \\ \alpha, \beta, \gamma, \delta \sim U(0, 1) \end{cases} \quad (33)$$

The offspring  $Q''$  is generated the same way by adjusting the airship sequence of  $P'$  according to  $Per_{i_0}$ .

For individuals that do not satisfy constraint (20) and (21), the repair operation is performed on them. The repair operation includes two operations: grouping and safety distance check. The grouping operation checks whether any two airships can communicate with each other. If not, all the airships are grouped into several groups according to the connections and one airship in the smallest group will be moved toward another

airship in the nearest group till they can communicate with each other. The safety distance check can identify the airships that are too close to the other airships according to constraint (20) and move them in the opposite direction till they reach a safety distance.

### C. Termination criterion

In [50], Saxena *et al.* proposed an entropy based termination criterion for MOEA. This termination criterion can terminate the iteration with high accuracy. A more important feature is that this criterion can trigger the termination as well when an MOEA falls into dilemma, and therefore it can partially reflect the performance of an MOEA. In this paper, the entropy based termination criterion is adopted as the termination criterion for all the experiments.

The process of the deployment optimization of NSCS using similarity-based MOEA/D is shown in Algorithm 1.

## V. EXPERIMENTS AND DISCUSSION

In this section, the proposed similarity-based MOEA/D for optimizing the deployment of NSCS is tested. We design five test problems of different features and the details of the five test problems are listed in Table II. All the circular hotspots, i.e., the circular urban areas, of the test problems are generated following Gaussian distribution. Four series of experiments are carried out. The first one is the test on shift initialization. The second is the test on the similarity-based reproduction operators. The third is the test on the similarity-based MOEA/D with shift initialization. The fourth is the test on two multiobjective evolutionary algorithm integrated with the similarity-based reproduction operators and shift initialization: the external archive guided multiobjective evolutionary algorithm based on decomposition (EAG-MOEA/D) [51] and the non-dominated sorting genetic algorithm II (NSGA-II) [52]. Each test instance is independently run for 10 times.

### A. Experimental results on shift initialization

The shift initialization is designed for working with the similarity-based MOEA/D. To test whether the shift initialization can improve the performance of the similarity-based MOEA/D, we test the shift initialization by comparing these two settings: the similarity-based MOEA/D using shift initialization (MOEA/D-SS) and the similarity-based MOEA/D using random initialization (MOEA/D-SR). We carry out the experiments on the five test problems with eight airships.

The area is 100 long and 100 wide. The airship altitude is 50 and the maximum communication range between airships is 20. The safety distance between the airships is 3. The radius of the projected coverage circle of each airship is 15, and the satellite's coverage is unlimited. The satellite is located at (50, 50, 300). The fading parameters  $E_f$  and  $E_r$  are  $6.3269 \times 10^{-6}$  and  $2.3148 \times 10^{-7}$  respectively. The capacity of each airship is 400, and so is the satellite. The demands of the urban users and the suburban users are 1.5 and 1 respectively. In shift initialization, each new individual copies one airship from the previously generated one. The weight

vectors are generated uniformly using the method described in [53]–[55]. The neighbor is 10% the size of the population. We use the penalty-based boundary intersection (PBI) [43] as the decomposition method, and the penalty factor is 1. We use the advised value in [50] for termination criterion. The probability of crossover is 0.7, and that of mutation is 0.3. The population size of the similarity-based MOEA/D using random initialization is the average of that using shift initialization. We use hypervolume to measure the quality of the Pareto front [56], [57].  $F$  test and  $t$  test are carried out with significance level of 0.05. The result is shown in Table III.

From Table III, we can notice that MOEA/D-SS outperforms MOEA/D-SR with better mean and standard deviation in single hotspot problem and L-shaped hotspot problem, and the significance tests show that the difference is significant. For the other problems, MOEA/D-SS and MOEA/D-SR have similar performance. The significance tests show that the difference is not significant both in mean and standard deviation. The reason is that the initial population structure is related with the hotspots. The initial neighbor individuals of single hotspot problem and L-shaped hotspot problem are more similar than those of the other three problems. There is only one hotspot in single hotspot problem and the area of the hotspots of L-shaped hotspot problem is large. This contributes to a less various neighbor solutions for these two problems. In contrast, the other three problems have more promising various solutions for a certain subproblem, which will weaken the search ability of the algorithm. The  $p$  values of  $t$  tests on the nine hotspots problem confirm this conclusion. From the analysis above, we can conclude that the shift initialization can enhance the similarity-based MOEA/D to some extent.

### B. Experimental results on similarity-based reproduction operators

Since the L-shaped hotspot problem combines the features of the other test problems, we test the similarity-based reproduction operators on L-shaped hotspot problem with 8 airships. We choose MOEA/D-DE with polynomial mutation [58], MOEA/D with simulated binary crossover and polynomial mutation (MOEA/D-SBX) [59], MOEA/D with blend crossover and uniform mutation (MOEA/D-BLX) [60] and MOEA/D with geometrical crossover and non-uniform mutation (MOEA/D-GC) [61] as comparisons. To test the actual performance of the operators, all the algorithms use the random initialization. The parameter  $F$  of differential operator is 0.5. The parameter  $\eta$  of SBX crossover is 1. The parameter  $\alpha$  of BLX crossover is 0.5. The other parameters are the same as in Section V-A. The result is shown in Table IV.

From Table IV, we can find out that the similarity-based MOEA/D with random initialization obtains better Pareto fronts than the other algorithms do. Although the standard deviation of MOEA/D-SR is the worst, the  $F$  tests show that the difference is not significant. This is mainly because the random initialization is unable to provide appropriately distributed initial population. If the random initialization happens to provide similar initialization as the shift initialization does, MOEA/D-SR will provide good result, and if a more randomized population is generated, MOEA/D-SR may be faced

TABLE II  
THE DETAIL OF THE FIVE TEST PROBLEMS

test problem	urban users	suburban users	motivation
single hotspot	4000	1000	elementary problem, to illustrate the basic behaviour of the optimization algorithms, the center is at (50,50), the radius is 30
double hotspots	2000(each hotspot)	1000	equilibrium problem, to illustrate how the algorithms weigh these two hotspots, the centers are at (30,30) and (70,70) respectively, all of the radii are 25
annulus	4000	1000	bridge problem, to illustrate the algorithms' ability to explore from inside to outside of the annulus or vice versa, and the perception ability is tested, all of the centers are at (50,50), the radii are 20 and 40 respectively
nine hotspots	450(each hotspot)	1000	exploration problem, to illustrate the algorithms' ability to find multiple hotspots, the centers are at (25,25), (50, 25), (75,25), (25,50), (50,50), (75,50), (25,75), (50,75) and (75,75) respectively, all of the radii are 10
L-shaped hotspot	2000 (L), 2000 (circle)	1000	general problem, combining the features of the above four problems and to illustrate the general performance of the algorithms, the vertices of the L-shaped hotspot are at (20,20), (20,80), (40,80), (40,40), (80,40) and (80,20) respectively, the center of the circular hotspot is at (70,70), the radius is 10

TABLE III  
THE MEAN AND STANDARD DEVIATION OF THE HYPERVOLUME OF SIMILARITY-BASED MOEA/D USING SHIFT INITIALIZATION AND SIMILARITY-BASED MOEA/D USING RANDOM INITIALIZATION

		single hotspot	double hotspots	annulus	nine hotspots	L-shaped hotspot
MOEA/D-SR	mean ( $\times 10^6$ )	4.2106	<b>4.2705</b>	4.1136	<b>4.5573</b>	4.2199
	std ( $\times 10^4$ )	1.8476	1.7957	<b>0.8874</b>	<b>1.6730</b>	1.4354
MOEA/D-SS	mean ( $\times 10^6$ )	<b>4.2440</b>	4.2581	<b>4.1148</b>	4.5500	<b>4.3209</b>
	std ( $\times 10^4$ )	<b>1.1016</b>	<b>1.1587</b>	1.2084	2.0688	<b>1.1450</b>
<i>F</i> test <i>p</i>		0.058	0.061	0.564	0.296	0.176
<i>t</i> test <i>p</i>		0	0.083	0.814	0.402	0
better <sup>1</sup>		<b>YES</b>	NO	NO	NO	<b>YES</b>

<sup>1</sup> this is the conclusion that whether MOEA/D-SS performs better than MOEA/D-SR.

TABLE IV  
THE MEAN AND STANDARD DEVIATION OF THE HYPERVOLUME OF MOEA/D-SR, MOEA/D-DE, MOEA/D-SBX, MOEA/D-BLX AND MOEA/D-GC

	mean	std	<i>F</i> test <i>p</i>	<i>t</i> test <i>p</i>	better <sup>1</sup>
MOEA/D-DE	4.1199	1.3575	0.198	0	<b>YES</b>
MOEA/D-SBX	4.1140	<b>1.0382</b>	0.055	0	<b>YES</b>
MOEA/D-BLX	4.1682	1.7700	0.427	0	<b>YES</b>
MOEA/D-GC	4.1705	1.6875	0.419	0	<b>YES</b>
MOEA/D-SR	<b>4.2313</b>	2.7527	NULL	NULL	NULL

<sup>1</sup> this is the conclusion that whether MOEA/D-SR performs better than the comparing algorithm.

with difficulty to perceive the latent regions. In conclusion, MOEA/D-SR outperforms the other algorithms with a high probability according to *t* test.

#### C. Experimental results on similarity-based MOEA/D using shift initialization

In this part, we test the performance of the similarity-based MOEA/D using shift initialization on all test problems. From the experiments in Section V-A and Section V-B, we can figure out that the similarity-based MOEA/D should work with shift initialization to maximize its effectiveness. Therefore we compare the performance of MOEA/D-SS, MOEA/D-DE,

MOEA/D-SBX, MOEA/D-BLX and MOEA/D-GC on all test problems with 4, 5, 6 and 8 airships. The parameters are the same as the tests in Section V-A and Section V-B. The results are shown in Fig. 5, 6, 7 and Table V, VI.

From Fig. 5, we notice the latent regions obtained by the algorithms. The algorithms only cover the latent regions while pay a little attention to the other parts of the area. This suggests that it is common for algorithms to have latent regions which likely contain the Pareto optimal solutions. The latent regions perceived by different algorithms are similar but not the same. The similar latent regions obtained by different algorithms means that they share a similar perception of where the airships are fully utilized. At the meantime, the algorithms evaluate each region differently. For example, in Fig. 5, both MOEA/D-SS and MOEA/D-DE regard region 1 and 2 as appropriate regions to deploy airships. However, MOEA/D-SS deploys airships to region 1 when considering coverage more than network speed, and deploys airships to region 2 when focusing on network speed. On the contrary, MOEA/D-DE considers region 1 as an appropriate location when focusing on both coverage and network speed, and pays less attention to region 2. From Table II, we can notice that the urban users are denser in region 2 than those in region 1, and it is clear that region 2 is a better region to deploy airships when focusing on network speed. The evaluation of region 1 and 2 indicates that MOEA/D-DE falls into local optima. Therefore it is important

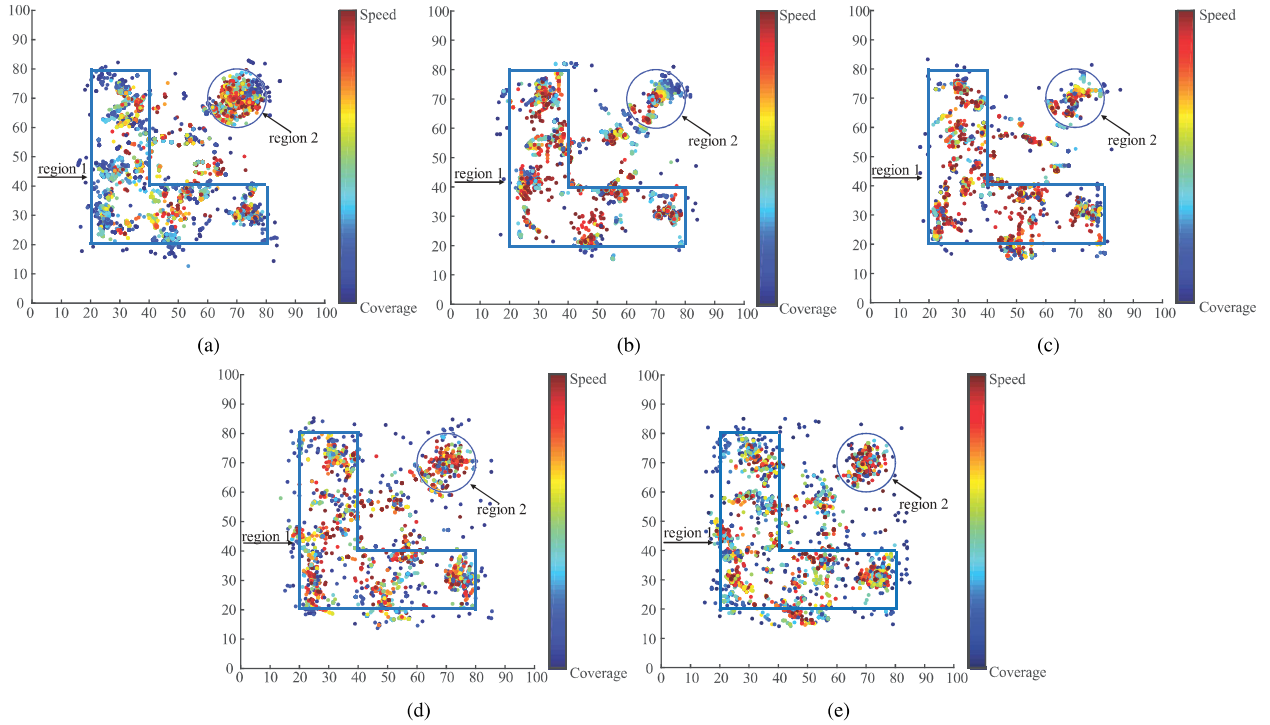


Fig. 5. The deployment of 8 airships of 10 repeated tests on L-shaped problem. The color of the airships ranges from blue to red corresponding to the subproblems from focusing on coverage to focusing on network speed. The airship deployment of each subgraph is obtained by (a) MOEA/D-SS, (b) MOEA/D-DE, (c) MOEA/D-SBX, (d) MOEA/D-BLX and (e) MOEA/D-GC.

for an algorithm to perceive the latent regions of the variable space and evaluate them correctly. It can be concluded that MOEA/D-SS succeeds in perceiving the latent regions and evaluating them correctly.

There are two reasons for the formation of the latent regions. First, different deployment regions, even though these regions have same number of users, have distinct impact on the performance of NSCS. Second, the safety and communication constraints make the airships keep a safety distance and maintain communication. These two aspects correspond to the objective functions and the constraints, which are the same for the other multiobjective optimization problems. For the other multiobjective optimization problems, the Pareto optimal solutions are located in a set of subspaces of the variable space, and the algorithm should perceive and evaluate these subspaces correctly to obtain a better result. Therefore MOEA/D-SS can be easily extended to the other multiobjective optimization problems.

From Fig. 6, it can be figured out that all the five algorithms obtain similar results when focusing on coverage, but MOEA/D-SS obtains better solutions than the other four algorithms do when focusing on network speed. This is because it is hard to deploy airships to promising locations without violating the constraints, which is the difficulty of this deployment optimization problem. The constraints make it more important that the algorithms should utilize the population's perception as much to generate new individuals as possible. The similarity-based MOEA/D redistributes airships among the latent regions and adjusts the positions of the airships inside a latent region while maintaining the perception integrity of the

population. Therefore the similarity-based MOEA/D performs better according to Fig. 6. And it can be concluded that the similarity-based MOEA/D can deploy airships more safely and appropriately. Therefore the similarity-based MOEA/D is more compatible with the constraints than the other algorithms.

From Fig. 7, we can notice that MOEA/D-SS converges faster than the other four algorithms do on all the problems except annulus. At the same time, the shift initialization can generate initial population of higher quality than the random initialization does. The initial population of high quality helps MOEA/D-SS converge faster.

The performance of the algorithms reflects the features of the test problems, and each test problem also examines some aspects of a algorithm's performance. In Table V, the percentage of mean to the best mean of a algorithm reflects the relative difficulty of this problem to this algorithm. If the mean of one algorithm on a test problem is far worse than the best mean, then this problem is relatively difficult to this algorithm. Therefore we can also use the averaged percentage of mean (APM) to reflect the relative difficulty of this test problem. According to APM in Table V, we can notice that the relative difficulty of the five problems from easy to difficult is: annulus, nine hotspots, single hotspot, double hotspots and L-shaped hotspot. We also use the averaged percentage of standard deviation (APSD) to reflect the stability of the algorithms on this problem.

The APM of the annulus problem is the highest of all the five test problems for all airship cases, and the APSD is small. This indicates that all the algorithms perform well on the annulus problem. This is due to the largest area of

TABLE V  
THE MEAN AND STANDARD DEVIATION OF THE HYPERVOLUME OF THE FIVE ALGORITHMS ON ALL TEST PROBLEMS

number of airships		single hotspot	double hotspots	annulus	nine hotspots	L-shaped hotspot	
4	MOEA/D-DE	mean ( $\times 10^6$ ) std ( $\times 10^4$ )	1.5799(99.4%) <sup>1</sup> 0.6092(273%) <sup>2</sup>	1.5865(98.5%) 0.6767(203%)	1.5431(99.7%) 0.2754(177%)	1.6523(99.6%) 0.2101(140%)	1.5582(97.5%) 2.2428(522%)
	MOEA/D-SBX	mean ( $\times 10^6$ ) std ( $\times 10^4$ )	1.5714(98.8%) 1.0820(486%)	1.5852(98.4%) 0.4754(143%)	1.5426(99.7%) 0.2476(159%)	1.6519(99.5%) 0.4893(326%)	1.5572(97.5%) 1.8562(432%)
	MOEA/D-BLX	mean ( $\times 10^6$ ) std ( $\times 10^4$ )	1.5822(99.5%) 0.4637(208%)	1.5999(99.3%) 0.8164(245%)	1.5446(99.8%) 0.1966(126%)	<b>1.6594(100%)</b> 0.2216(147%)	1.5738(98.5%) 2.4883(579%)
	MOEA/D-GC	mean ( $\times 10^6$ ) std ( $\times 10^4$ )	1.5823(99.5%) 0.3232(145%)	1.6002(99.4%) 0.4019(121%)	1.5446(99.8%) <b>0.1555(100%)</b>	1.6577(99.9%) <b>0.1503(100%)</b>	1.5681(98.1%) 2.0158(469%)
	MOEA/D-SS	mean ( $\times 10^6$ ) std ( $\times 10^4$ )	<b>1.5900(100%)</b> <b>0.2228(100%)</b>	<b>1.6105(100%)</b> <b>0.3326(100%)</b>	<b>1.5471(100%)</b> 0.1562(100%)	<b>1.6594(100%)</b> 0.4978(331%)	<b>1.5978(100%)</b> <b>0.4294(100%)</b>
		APM <sup>3</sup>	99.3%	98.9%	99.8%	99.8%	97.9%
		APSD <sup>4</sup>	278%	178%	140%	236%	501%
	MOEA/D-DE	mean ( $\times 10^6$ ) std ( $\times 10^4$ )	2.1208(98.8%) 0.7608(259%)	2.1063(97.1%) 2.7009(310%)	2.0819(99.7%) 0.4165(185%)	2.2366(98.7%) 1.8231(1102%)	2.0957(96.9%) 1.8029(322%)
	MOEA/D-SBX	mean ( $\times 10^6$ ) std ( $\times 10^4$ )	2.0882(97.3%) 1.8843(641%)	2.1007(96.9%) 3.1399(361%)	2.0782(99.5%) 0.3659(163%)	2.2372(98.7%) 1.4410(871%)	2.0862(96.4%) 0.8853(158%)
	MOEA/D-BLX	mean ( $\times 10^6$ ) std ( $\times 10^4$ )	2.1247(99.0%) 1.4858(505%)	2.1393(98.7%) 1.3380(154%)	2.0867(99.9%) <b>0.2241(100%)</b>	2.2648(99.9%) 0.3177(192%)	2.1201(98%) 2.2997(411%)
5	MOEA/D-GC	mean ( $\times 10^6$ ) std ( $\times 10^4$ )	2.1275(99.1%) 0.8204(279%)	2.1478(99.1%) 1.1764(135%)	<b>2.0880(100%)</b> 0.3481(155%)	2.2641(99.9%) 0.2799(169%)	2.0955(96.9%) <b>0.5595(100%)</b>
	MOEA/D-SS	mean ( $\times 10^6$ ) std ( $\times 10^4$ )	<b>2.1459(100%)</b> <b>0.2940(100%)</b>	<b>2.1681(100%)</b> <b>0.8704(100%)</b>	2.0876(100%) 0.2542(113%)	<b>2.2656(100%)</b> <b>0.1654(100%)</b>	<b>2.1632(100%)</b> 0.9588(171%)
		APM	98.6%	98.0%	99.8%	99.3%	97.1%
		APSD	421%	240%	154%	583%	266%
	MOEA/D-DE	mean ( $\times 10^6$ ) std ( $\times 10^4$ )	2.7331(98.3%) 1.5836(493%)	2.7144(96.9%) 3.5512(516%)	2.6854(99.5%) 0.3453(155%)	2.9186(98.7%) 1.5233(224%)	2.6973(95.8%) 1.7199(195%)
	MOEA/D-SBX	mean ( $\times 10^6$ ) std ( $\times 10^4$ )	2.7015(97.1%) 1.1806(359%)	2.6905(96.0%) 1.2090(176%)	2.6852(99.5%) 0.6220(280%)	2.9073(98.3%) 1.5029(221%)	2.6896(95.5%) <b>0.8833(100%)</b>
	MOEA/D-BLX	mean ( $\times 10^6$ ) std ( $\times 10^4$ )	2.7423(98.6%) 1.0970(333%)	2.7320(97.5%) <b>0.6880(100%)</b>	2.6954(99.9%) <b>0.2222(100%)</b>	2.9422(99.5%) 0.8688(128%)	2.7246(96.8%) 1.4551(165%)
	MOEA/D-GC	mean ( $\times 10^6$ ) std ( $\times 10^4$ )	2.7442(98.7%) 1.1212(341%)	2.7390(97.8%) 1.1536(168%)	2.6971(99.9%) 0.2451(110%)	2.9506(99.8%) 1.0200(150%)	2.7345(97.1%) 1.4835(168%)
	MOEA/D-SS	mean ( $\times 10^6$ ) std ( $\times 10^4$ )	<b>2.7813(100%)</b> <b>0.3290(100%)</b>	<b>2.8020(100%)</b> 1.5040(219%)	<b>2.6993(100%)</b> 0.3909(176%)	<b>2.9569(100%)</b> <b>0.6808(100%)</b>	<b>2.8152(100%)</b> 2.4469(277%)
		APM	98.2%	97.1%	99.7%	99.1%	96.3%
		APSD	381%	270%	180%	181%	201%
8	MOEA/D-DE	mean ( $\times 10^6$ ) std ( $\times 10^4$ )	4.1453(97.8%) 2.3287(280%)	4.1328(97.1%) 1.8196(130%)	4.0761(99.0%) 0.9595(118%)	4.4893(98.5%) 2.8459(166%)	4.1175(95.5%) 1.1522(128%)
	MOEA/D-SBX	mean ( $\times 10^6$ ) std ( $\times 10^4$ )	4.0877(96.4%) 1.6241(195%)	4.1233(96.8%) 2.2208(159%)	4.0716(98.9%) 1.0339(127%)	4.4760(98.2%) 2.8364(165%)	4.1099(95.3%) <b>0.9000(100%)</b>
	MOEA/D-BLX	mean ( $\times 10^6$ ) std ( $\times 10^4$ )	4.1237(97.3%) 1.1314(136%)	4.1528(97.5%) 1.6705(120%)	4.1055(99.7%) <b>0.8120(100%)</b>	4.4871(98.4%) 2.1053(123%)	4.1572(96.4%) 1.8906(210%)
	MOEA/D-GC	mean ( $\times 10^6$ ) std ( $\times 10^4$ )	4.1460(97.8%) 1.4359(172%)	4.1733(98.0%) <b>1.3948(100%)</b>	4.1091(99.8%) 1.0422(128%)	4.4953(98.6%) 2.1903(128%)	4.1564(96.4%) 1.8785(208%)
	MOEA/D-SS	mean ( $\times 10^6$ ) std ( $\times 10^4$ )	<b>4.2392(100%)</b> <b>0.8327(100%)</b>	<b>4.2577(100%)</b> 1.4508(104%)	<b>4.1166(100%)</b> 1.2738(157%)	<b>4.5580(100%)</b> <b>1.7143(100%)</b>	<b>4.3109(100%)</b> 1.6724(186%)
		APM	97.3%	97.3%	99.4%	98.4%	95.9%
		APSD	196%	128%	132%	146%	183%

<sup>1</sup> For each algorithm, this is the percentage of the current mean to the best mean in the case of the current test problem and airships.

<sup>2</sup> For each algorithm, this is the percentage of the current standard deviation to the best standard deviation in the case of the current test problem airships.

<sup>3</sup> This is the averaged percentage of the current mean to the best mean (APM) in the case of the current test problem and airships, the best mean value of the current test problem is not counted.

<sup>4</sup> This is the averaged percentage of the current standard deviation to the best standard deviation (APSD) in the case of the current test problem, the best standard deviation of the current test problem is not counted.

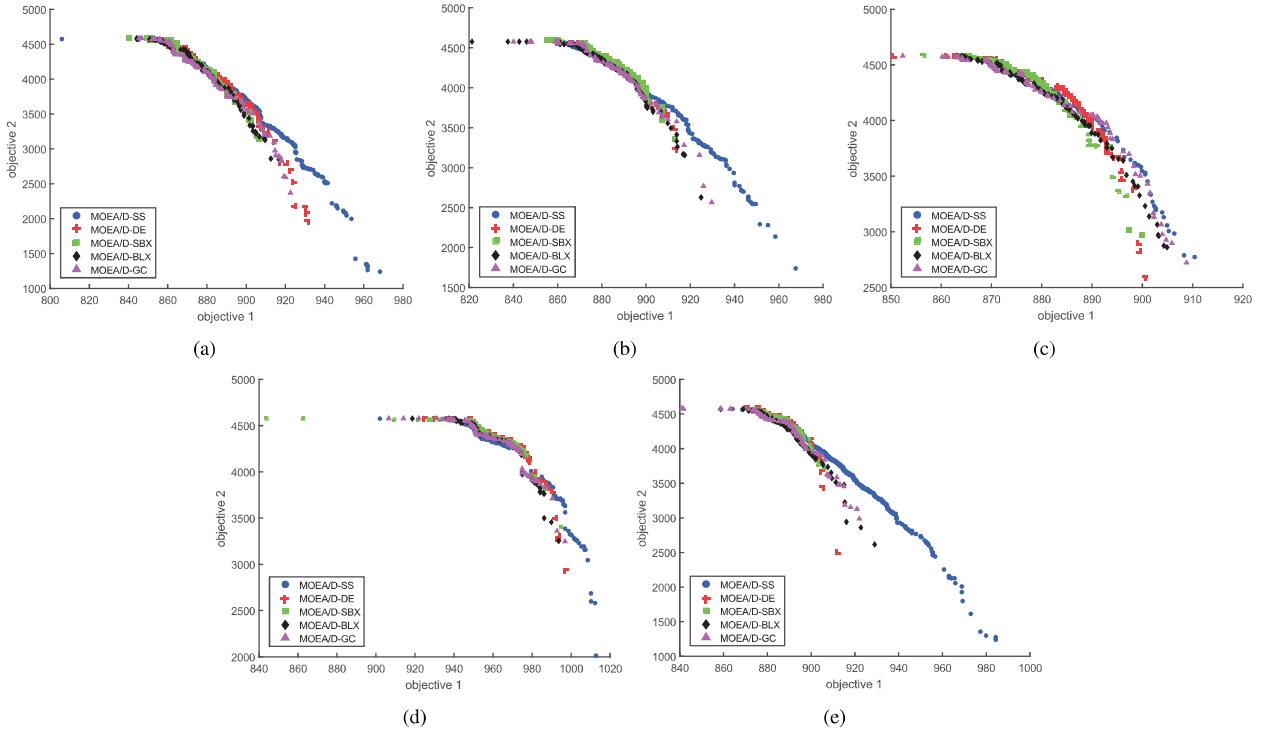


Fig. 6. The integrated Pareto fronts of 8 airships on the five test problems. Each Pareto front is obtained by combining the Pareto optimal solutions of 10 repeated tests which are selected according to the domination relationship. The test problem that each subgraph corresponds to is: (a) single hotspot, (b) double hotspots, (c) annulus, (d) nine hotspots and (e) L-shaped hotspot.

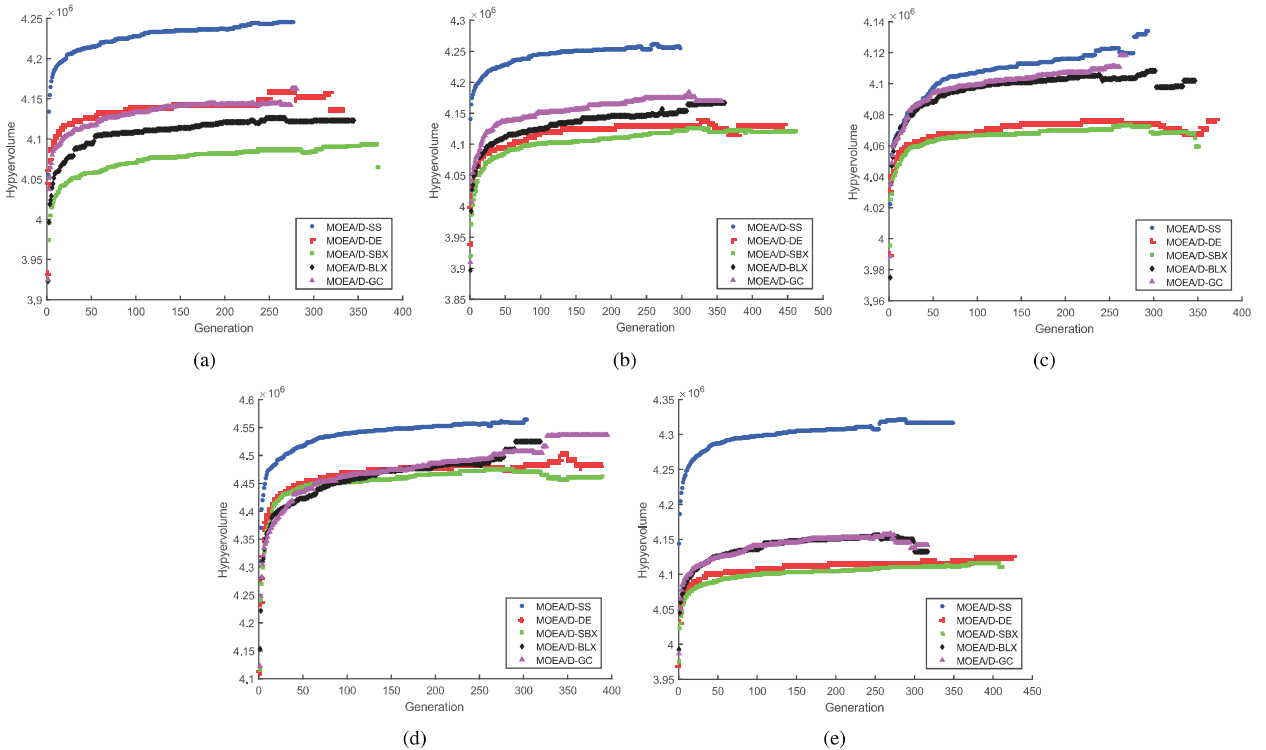


Fig. 7. The averaged hypervolume against generation of 8 airships on the five test problems. The averaged hypervolume of each generation is averaged using the hypervolume of that generation of 10 repetition tests. Only those tests that have hypervolume in that generation can participate the calculation. The corresponding test problem of each subgraph is: (a) single hotspot, (b) double hotspots, (c) annulus, (d) nine hotspots and (e) L-shaped hotspot.

the hotspot and the sparest urban user distribution. The large hotspot provides the algorithms with many optional similar

TABLE VI  
THE  $p$  VALUES OF  $t$  TESTS AND THE COMPARISON CONCLUSION OF THE FOUR ALGORITHMS AGAINST MOEA/D-SS

number of airships		single hotspot	double hotspots	annulus	nine hotspots	L-shaped hotspot
4	MOEA/D-DE	$t$ test $p$	0	0.001	0.001	0
		better	<b>YES</b>	<b>YES</b>	<b>YES</b>	<b>YES</b>
	MOEA/D-SBX	$t$ test $p$	0	0	0.003	0
		better	<b>YES</b>	<b>YES</b>	<b>YES</b>	<b>YES</b>
	MOEA/D-BLX	$t$ test $p$	0	0	0.006	0.965
		better	<b>YES</b>	<b>YES</b>	NO	<b>YES</b>
	MOEA/D-GC	$t$ test $p$	0	0.003	0.002	0.304
		better	<b>YES</b>	<b>YES</b>	NO	<b>YES</b>
5	MOEA/D-DE	$t$ test $p$	0	0	0.002	0.01
		better	<b>YES</b>	<b>YES</b>	<b>YES</b>	<b>YES</b>
	MOEA/D-SBX	$t$ test $p$	0	0	0	0
		better	<b>YES</b>	<b>YES</b>	<b>YES</b>	<b>YES</b>
	MOEA/D-BLX	$t$ test $p$	0	0	0.378	0.491
		better	<b>YES</b>	<b>YES</b>	NO	<b>YES</b>
	MOEA/D-GC	$t$ test $p$	0	0	0.768	0.176
		better	<b>YES</b>	<b>YES</b>	NO	<b>YES</b>
6	MOEA/D-DE	$t$ test $p$	0	0	0	0
		better	<b>YES</b>	<b>YES</b>	<b>YES</b>	<b>YES</b>
	MOEA/D-SBX	$t$ test $p$	0	0	0	0
		better	<b>YES</b>	<b>YES</b>	<b>YES</b>	<b>YES</b>
	MOEA/D-BLX	$t$ test $p$	0	0	0.014	0.001
		better	<b>YES</b>	<b>YES</b>	<b>YES</b>	<b>YES</b>
	MOEA/D-GC	$t$ test $p$	0	0	0.161	0.124
		better	<b>YES</b>	<b>YES</b>	NO	<b>YES</b>
8	MOEA/D-DE	$t$ test $p$	0	0	0	0
		better	<b>YES</b>	<b>YES</b>	<b>YES</b>	<b>YES</b>
	MOEA/D-SBX	$t$ test $p$	0	0	0	0
		better	<b>YES</b>	<b>YES</b>	<b>YES</b>	<b>YES</b>
	MOEA/D-BLX	$t$ test $p$	0	0	0.032	0
		better	<b>YES</b>	<b>YES</b>	<b>YES</b>	<b>YES</b>
	MOEA/D-GC	$t$ test $p$	0	0	0.163	0
		better	<b>YES</b>	<b>YES</b>	NO	<b>YES</b>

regions, which lowers the difficulty. The difficulty of the annulus problem is that the sparse urban users make urban area and suburban area more indistinct, which can examine the perception ability of the algorithms. From Table VI, we notice that MOEA/D-SS significantly outperforms the other algorithms with 4 airships. MOEA/D-SS and MOEA/D-GC outperform the other algorithms with 5, 6 and 8 airships. The  $t$  tests on the annulus problem show that MOEA/D-SS has a good ability of detecting the hotspots and perceiving the decision variable space.

The nine hotspots problem is more difficult than the annulus problem. The hotspots of the nine hotspots problem are small and have dense urban users. Therefore the algorithms have many optional regions to deploy the airships. However, these optional regions make the individuals of each subproblem's neighbors diverse, which means that the two parents may be quite different. This increases the difficulty for MOEA/D-SS to pair the airships of two parents especially with fewer airships. Thus this problem can examine the stability of MOEA/D-SS. From Table VI, we notice that MOEA/D-SS achieves the best mean and standard deviation in all airship cases. MOEA/D-SS achieves the best stan-

dard deviation as well except with 4 airships. From Table VI, it can be figured out that the probability  $p$  of  $t$  test drops with more airships deployed, which means that the performance gap between MOEA/D-SS and the other algorithms becomes larger. Therefore we can figure it out that the similarity-based MOEA/D performs well in tracking multiple hotspots, which means that the similarity-based MOEA/D is stable even though the individuals of neighbors are diverse.

The difficulty of the single hotspot problem comes from the fact that there is only one hotspot and the users are relatively concentrated. To obtain high network speed, the algorithms should deploy many airships around the only hotspot, which rises the difficulty in satisfying constraint (20). To improve the quality of the solutions, the algorithms should generate offsprings that need as less repair operation as possible so that the offspring quality will not be deteriorated too much. Thus this problem reflects the compatibility between the reproduction operators and the constraints. From Table V and VI, we can notice that MOEA/D-SS achieves the best mean and standard deviation in all airship cases, and outperforms the other algorithms significantly. The result indicates that

MOEA/D-SS can deploy airships more safely and appropriately, which means that MOEA/D-SS are more compatible with the constraints.

Compared with the single hotspot problem, the double hotspots problem increases the difficulty by adding one hotspot. The APM and APSD are smaller than those of the single hotspot problem in every cases. This indicates that it is difficult for the algorithms to strike a balance between the two hotspots, but the two hotspots provide algorithms with more optional regions to stabilize the performance. This problem requires the algorithms to make big changes for each individual by redistributing airships between these two hotspots, and these changes must be effective and efficient. Again, this problem emphasizes the correctness and importance of the population's perception. In 4 and 5 airships cases, MOEA/D-SS is the most stable algorithm. In 6 and 8 airships cases, the redistribution of airships between the two hotspots incurs fluctuation in the performance of MOEA/D-SS, but MOEA/D-SS achieves the best mean in all cases. From Table. VI, we can figure out that MOEA/D-SS significantly outperforms the other algorithms on this problem, and this problem testifies the effectiveness and efficiency of the similarity-based MOEA/D.

The L-shaped hotspot problem combines the features of the previous four test problems. The L-shaped hotspot has relatively sparse urban users and large area. The urban users are denser in the circular hotspot, which makes it the best location to deploy airships to get high network speed. The algorithms should evaluate these two hotspots correctly. The complexity of this problem results in small APM and large APSD as shown in Table V. MOEA/D-SS achieves the best mean in all cases but is not the most stable one. According to Table VI, MOEA/D-SS outperforms the other algorithms significantly in all cases on this problem.

By now, all the discussion is limited to a two objective problem. For problems with many objectives, the evolutionary process is easily stuck in a situation where almost all individuals are non-dominated. To overcome this defect, one way is to find promising search directions so that dominating solutions can be generated. The proposed algorithm matches the perceptions of different individuals about the whole decision variable space, which is an objective dimension independent process. The similarity-based approach adaptively divides the high dimensional space into latent regions according to the similarity between two individuals. According to the perceptions of specific individuals, the promising directions are different inside latent regions and among different regions. The calculation of the promising directions is independent of the number of objectives as well. With perception comparison process, the two individuals work together to search the promising areas, which reduces the search space to some extent. In summary, the proposed similarity-based MOEA/D is an objective independent algorithm and can be utilized to solve MOP with many objectives.

#### *D. Experimental results on similarity-based EAG-MOEA/D and NSGA-II with shift initialization*

In order to test the performance of the proposed similarity-based reproduction scheme and shift initialization integrated

with the other algorithms, we combine the proposed scheme with EAG-MOEA/D and NSGA-II. EAG-MOEA/D maintains an external archive which is selected based on the non-dominated sorting. Each subproblem's successful rate of its offsprings entering the external archive is calculated and used to select corresponding subproblems to produce new offsprings. NSGA-II uses a non-dominated sorting to select the next generation. All the two algorithms use the same parameters as MOEA/D-SS does. The generations for calculating successful rate in EAG-MOEA/D-SS is 8 as suggested in [51]. To validate the effectiveness of the proposed similarity-based reproduction scheme and shift initialization, four algorithms are tested for EAG-MOEA/D and NSGA-II. For EAG-MOEA/D-SS, the four algorithms are: EAG-MOEA/D-DE with polynomial mutation (EAG-MOEA/D-DE), EAG-MOEA/D with simulated binary crossover and polynomial mutation (EAG-MOEA/D-SBX), EAG-MOEA/D with blend crossover and uniform mutation (EAG-MOEA/D-BLX) and EAG-MOEA/D with geometrical crossover and non-uniform mutation (EAG-MOEA/D-GC). For NSGA-II-SS, the four algorithms are: NSGA-II with differential operator and polynomial mutation (NSGA-II-DE), NSGA-II with simulated binary crossover and polynomial mutation (NSGA-II-SBX), NSGA-II with blend crossover and uniform mutation (NSGA-II-BLX) and NSGA-II with geometrical crossover and non-uniform mutation (NSGA-II-GC). The results are shown in Table VII, VIII, IX, Fig. 8, 9, 10 and 11.

From Table VII and VIII, we can notice that EAG-MOEA/D-SS and NSGA-II-SS perform significantly better than the algorithms combined with the other reproduction operators and random initialization from the perspective of hypervolume. This indicates that the proposed similarity-based reproduction operators work well with the other algorithms. This is due to the independency of the similarity-based reproduction scheme, which is performed in an individual level. EAG-MOEA/D-SS has similar performance with EAG-MOEA/D-SBX and EAG-MOEA/D-GC. Even though MOEA/D-SS does not outperform MOEA/D-SBX and MOEA/D-GC with a significance level of 0, it performs better than EAG-MOEA/D-SS does. This is due to the parent selection scheme of EAG-MOEA/D-SS. In EAG-MOEA/D-SS, the parents for reproduction are selected based on their performance in the last generations. This works well for those problems that have a relatively small optimal regions of decision variable. However, it is not the same for the deployment optimization of NSCS. For deployment optimization of NSCS, there are many latent promising regions. NSCS can provide a high network speed or cover a large area by assigning different number of airships and adjusting their positions in a same region. Thus it is not hard for a subproblem to generate good offsprings, and MOEA/D-SS maintains the perception of the whole area better. The parent selection scheme in EAG-MOEA/D-SS limits the search capability of some subproblems while providing the good solutions with more opportunity. From the analysis above, we can conclude that it is necessary to assign balanced computation resource for MOPs whose subproblems have large probability generating good offsprings, and the deployment optimization of NSCS is

TABLE VII

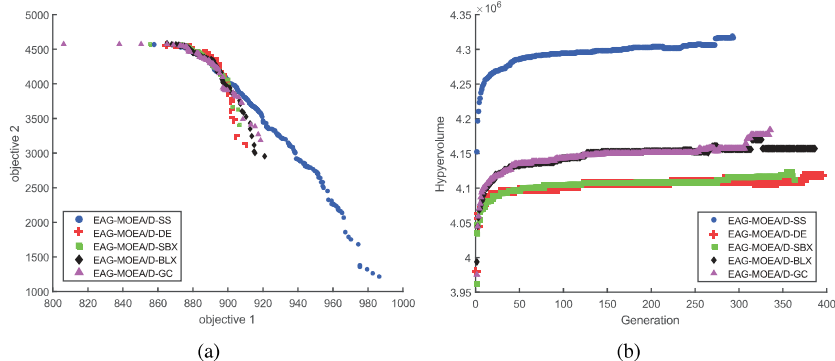
THE  $p$  VALUES OF  $t$  TESTS AND THE COMPARISON CONCLUSION OF FOUR EAG-MOEA/D BASED ALGORITHMS AGAINST EAG-MOEA/D-SS WITH 8 AIRSHIPS

number of airships		single hotspot	double hotspots	annulus	nine hotspots	L-shaped hotspot
8	EAG-MOEA/D-DE	$t$ test $p$	0	0	0	0
		better	YES	YES	YES	YES
	EAG-MOEA/D-SBX	$t$ test $p$	0	0	0	0
		better	YES	YES	YES	YES
	EAG-MOEA/D-BLX	$t$ test $p$	0	0	0.809	0
		better	YES	YES	NO	YES
	EAG-MOEA/D-GC	$t$ test $p$	0	0	0.921	0
		better	YES	YES	NO	YES

TABLE VIII

THE  $p$  VALUES OF  $t$  TESTS AND THE COMPARISON CONCLUSION OF FOUR NSGA-II BASED ALGORITHMS AGAINST NSGA-II-SS WITH 8 AIRSHIPS

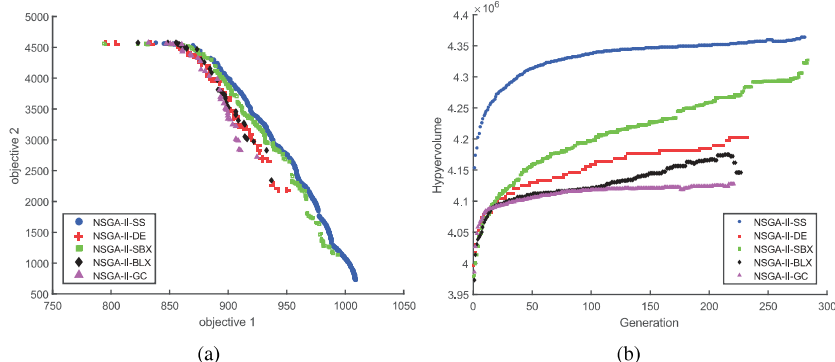
number of airships		single hotspot	double hotspots	annulus	nine hotspots	L-shaped hotspot
8	NSGA-II-DE	$t$ test $p$	0	0	0	0
		better	YES	YES	YES	YES
	NSGA-II-SBX	$t$ test $p$	0	0	0	0
		better	YES	YES	YES	YES
	NSGA-II-BLX	$t$ test $p$	0	0	0	0
		better	YES	YES	YES	YES
	NSGA-II-GC	$t$ test $p$	0	0	0	0
		better	YES	YES	YES	YES



(a)

(b)

Fig. 8. The integrated Pareto fronts and hypervolumes for 8 airships on L-shaped problem obtained by EAG-MOEA/D. Each Pareto front is obtained by combining the Pareto optimal solutions of 10 repeated tests which are selected according to the domination relationship. The averaged hypervolume of each generation is averaged using the final hypervolumes 10 repeated tests. (a). The integrated Pareto fronts. (b) The hypervolumes



(a)

(b)

Fig. 9. The integrated Pareto fronts and hypervolumes for 8 airships on L-shaped problem obtained by NSGA-II. Each Pareto front is obtained by combining the Pareto optimal solutions of 10 repeated tests which are selected according to the domination relationship. The averaged hypervolume of each generation is averaged using the final hypervolumes 10 repeated tests. (a). The integrated Pareto fronts. (b) The hypervolumes

such a problem.

According to Fig. 8 (a) and Fig. 9 (a), we can notice that EAG-MOEA/D-SS and NSGA-II-SS perform well in obtaining different parts of the Pareto front. This means that both of them can not only deploy airships around hotspots well and maintain good routing efficiency but also cover a large area. In Fig 9, the comparison algorithms optimize the first objective better than those of MOEA/D and EAG-MOEA/D do. This results from the fact that NSGA-II does not have a subproblem structure. This results in a population with a more common perception which helps to find better solutions when considering the first objective more than the second objective. Thus we can notice that all the NSGA-II based algorithms do better for the first objective. In Fig. 8 and 9, the shift initialization helps EAG-MOEA/D-SS and NSGA-II-SS converge fast.

In Fig. 10, 11 and Table IX, we compare the performance of MOEA/D-SS, EAG-MOEA/D-SS and NSGA-II-SS. From Fig. 10 (a), we notice that the Pareto fronts of MOEA/D-SS and EAG-MOEA/D-SS are similar, but NSGA-II-SS falls into local optima around the inflection point and finds less solutions. This is due to the many hotspots in nine hotspots problem. As we have discussed above, the non-subproblem structure of NSGA-II has the perception of a certain region being transferred through the whole population easily and thus a more common perception is formed in the population. This makes it easier in finding optimal position around hotspots. However, this non-subproblem structure does not allocate as even search resource for two objectives as MOEA/D-SS and EAG-MOEA/D-SS do. On the contrary, MOEA/D-SS and EAG-MOEA/D pay more even attention to different tradeoffs of the two objectives. Therefore MOEA/D-SS and EAG-MOEA/D-SS have a even performance when considering these two objectives. The same phenomenon exists for L-shaped hotspot problems as well.

Results from more effort on the first objective, the hypervolume obtained by NSGA-II-SS is higher than MOEA/D-SS and EAG-MOEA/D-SS as shown in Fig. 11. The hypervolume difference between NSGA-II-SS and MOEA/D-SS, EAG-MOEA/D-SS is small for nine hotspots problem, but large for L-shaped hotspot problem. This is because there are much more hotspots in nine hotspots problem, and the size of hotspots is smaller. More hotspots with denser users make the population's perceptions more diverse, which is suitable for the subproblem structure of MOEA/D-SS and EAG-MOEA/D-SS to deal with. However, NSGA-II-SS obviously achieves a better hypervolume than the other two algorithms for L-shaped hotspot, because there are just two hotspots and the user density is smaller. Compare the results from Fig. 10 and 11, we can notice that though NSGA-II-SS can achieve a better hypervolume, the comparison among these three algorithms actually depends on objective tradeoff. NSGA-II performs well in finding optimal positions around hotspots while MOEA/D-SS and EAG-MOEA/D are good at striking a balance between network speed and coverage.

According to Table IX, we can notice that MOEA/D-SS achieves a significantly better hypervolume than EAG-MOEA/D-SS for double hotspots problem and nine hotspots

problem. NSGA-II achieves better hypervolume for all problems except nine hotspots problem. However, all the three algorithms have their drawbacks. MOEA/D-SS and EAG-MOEA/D maintain a balance in various tradeoffs between two objectives while NSGA-II-SS is good at finding better locations around hotspots. Thus there is a potential that we can combine the advantages of these three algorithms.

According to the analysis above, we can provide some suggestions for the deployment related optimization problems. First, it is helpful to classify the perceptions of different individuals like the neighborhood structure in MOEA/D. Second, a more evenly distributed computation resource is preferred for deployment optimization problems whose optimal space of decision variable is large. Third, a small penalty factor for PBI or a dynamic weight adjustment scheme may help find better solutions around regions of interest after several generations.

## VI. CONCLUDING REMARKS

In this section, we will conclude the content of this paper and propose the challenges and the future work. In this paper, we first analyze the newest progress of deployment optimization in sensor network, smart grid, cellular network and NSCS. The relations and differences are analyzed between NSCS and other networks. Then we propose a multiobjective deployment optimization model considering the important aspects of NSCS and the other networks. Based on the features of the deployment optimization problem, we propose a similarity-based MOEA/D which utilizes the population's perception to recognize and evaluate the variable space. The *t* tests show that the similarity-based MOEA/D outperforms the other algorithms significantly in most cases. The similarity-based reproduction scheme is also tested on the other popular algorithms and the results validate its effectiveness. A suggestion is also given for solving the other deployment related optimization problems.

In the future work, we will continue on these challenges:

- We will apply the similarity-based MOEA/D to the other multiobjective optimization problems to investigate their perception structures.
- A framework combines the advantages of MOEA/D and NSGA-II will be developed to improve the performance.
- We will try to optimize the deployment of large-scale NSCS to study the performance of the proposed algorithm.

## REFERENCES

- [1] M. C. Ozdemir, "Conceptual changes by use of near space," in *Proc. 32nd IEEE/AIAA Conf. Digital Avionics Syst.*, NewYork, NY, USA, 2013, pp. 1–30.
- [2] M. A. Xapsos, P. M. O'Neill, and T. P. O'Brien, "Near-earth space radiation models," *IEEE Trans. Nucl. Sci.*, vol. 60, no. 3, pp. 1691–1705, Jun. 2013.
- [3] X. Qin, W. Zhan, J. ZhiHong, and H. Kan, "A miniature HRWS SAR concept for near-space vehicles," in *Proc. 13th Int. Symp. Radar*, Warsaw, Poland, May 2012, pp. 292–295.
- [4] H. Yang, Z. Li, J. Wu, Y. Huang, J. Yang, and X. Yang, "Near-space slow SAR high-resolution and wide-swath imaging concepts," in *Proc. IEEE Conf. Radar*, Ottawa, ON, Canada, 2013, pp. 1–5.
- [5] Y. Yang, J. Wu, Y. Xie, and W. Zheng, "Dynamics modeing and maneuverability analysis of a near-space earth observation platform," in *Proc. 5th Int. Conf. Recent Advances in Space Technol.*, Istanbul, Turkey, 2011, pp. 223–226.

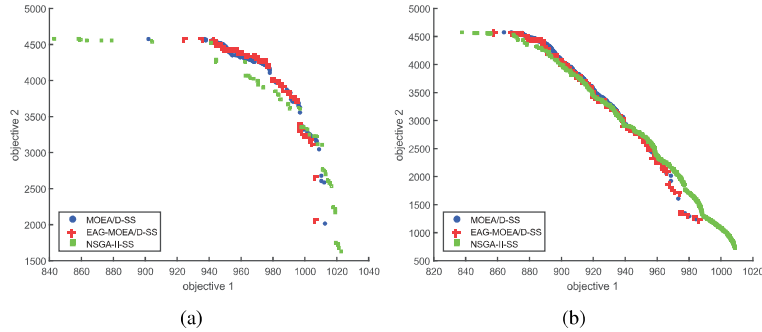


Fig. 10. The integrated Pareto fronts obtained by MOEA/D-SS, EAG-MOEA/D-SS and NSGA-II-SS. (a). Pareto fronts of 8 airships on nine hotspots problem. (b). Pareto fronts of 8 airships on L-shaped hotspot problem.

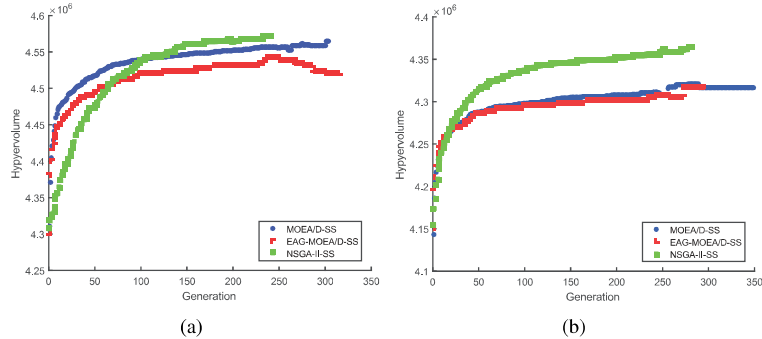


Fig. 11. The hypervolumes obtained by MOEA/D-SS, EAG-MOEA/D-SS and NSGA-II-SS. (a). Hypervolumes of 8 airships on nine hotspots problem. (b). Hypervolumes of 8 airships on L-shaped hotspot problem.

TABLE IX  
THE  $p$  VALUES OF  $t$  TESTS AND THE COMPARISON CONCLUSION OF EAG-MOEA/D-SS AND NSGA-II-SS AGAINST MOEA/D-SS

number of airships		single hotspot	double hotspots	annulus	nine hotspots	L-shaped hotspot
8	EAG-MOEA/D-SS	$t$ test $p$ the better one <sup>1</sup>	0.798	0.012	0.08	0.006
			-	<b>P</b>	-	<b>P</b>
	NSGA-II-SS	$t$ test $p$ the better one	0	0	0	0.85
			<b>N</b>	<b>N</b>	<b>N</b>	<b>N</b>

<sup>1</sup> This row shows the  $t$  test conclusion. ‘P’ stands for the proposed MOEA/D-SS is significantly better than the compared algorithm. ‘N’ stands for that the NSGA-II-SS is significantly better than MOEA/D-SS. ‘-’ stands for that the compared algorithms have no significant difference.

- [6] M. Guan, Q. Guo, and L. Lu, “A novel access protocol for communication system in near space,” in *Proc. Int. Conf. Wireless Commun., Networking and Mobile Computing*, Shanghai, China, 2007, pp. 1849–1852.
- [7] G. M. Djuknic, J. Freidenfelds, and Y. Okunev, “Establishing wireless communications services via high-altitude aeronautical platforms: a concept whose time has come?” *IEEE Commun. Mag.*, vol. 35, no. 9, pp. 128–135, Sep. 1997.
- [8] X. Wang, X. Gao, R. Zong, and P. Cheng, “An optimal model and solution of deployment of airships for high altitude platforms,” in *Proc. Int. Conf. Wireless Commun. and Signal Process.*, Suzhou, China, 2010, pp. 1–6.
- [9] X. Wang, X. Gao, and R. Zong, “Energy-efficient deployment of airships for high altitude platforms: A deterministic annealing approach,” in *Proc. IEEE Conf. Global Telecommun.*, Houston, TX, USA, 2011, pp. 1–6.
- [10] Y. Yin and S. Huang, “Optimization deployment of multi-sensor platforms in near-space based on adaptive genetic algorithm,” in *Proc. Int. Conf. Inform. Eng. and Comput. Sci.*, Wuhan, China, 2009, pp. 1–5.
- [11] Z. Wang, M. Gong, Q. Cai, L. Ma, and L. Jiao, “Deployment optimization of near space airships based on MOEA/D with local search,” in *Proc. IEEE Congr. on Evol. Comput.*, Beijing, China, 2014, pp. 2345–2352.
- [12] M. Hefeeda and M. Bagheri, “Forest fire modeling and early detection using wireless sensor networks,” *Ad Hoc Sensor Wireless Netw.*, vol. 7, no. 3, pp. 169–224, Jul. 2009.
- [13] Y. Xu and X. Yao, “A GA approach to the optimal placement of sensors in wireless sensor networks with obstacles and preferences,” in *Proc. 3rd IEEE Consum. Commun. and Netw. Conf.*, vol. 1, 2006, pp. 127–131.
- [14] M. R. Ingle and N. Bawane, “An energy efficient deployment of nodes in wireless sensor network using Voronoi diagram,” in *Proc. 3rd Int. Conf. Electron. Comput. Technol.*, Kanyakumari, India, Apr. 2011, pp. 307–311.
- [15] Y. Mohamed and A. Kemal, “Strategies and techniques for node placement in wireless sensor networks: A survey,” *Ad Hoc Netw.*, vol. 6, no. 4, pp. 621–655, Jun. 2008.
- [16] R. C. Luo and O. Chen, “Mobile sensor node deployment and asynchronous power management for wireless sensor networks,” *IEEE Trans. Ind. Electron.*, vol. 59, no. 5, pp. 2377–2385, Mar. 2012.
- [17] Z. Yun, X. Bai, D. Xuan, W. Jia, and W. Zhao, “Pattern mutation in wireless sensor deployment,” *IEEE/ACM Trans. Netw.*, vol. 20, no. 6, pp. 1964–1977, Dec. 2012.
- [18] S. He, X. Gong, J. Zhang, J. Chen, and Y. Sun, “Curve-based deployment for barrier coverage in wireless sensor networks,” *IEEE Trans. Wireless Commun.*, vol. 13, no. 2, pp. 724–735, Feb. 2014.
- [19] S. Temel, N. Unaldi, and O. Kaynak, “On deployment of wireless sensors on 3-d terrains to maximize sensing coverage by utilizing cat swarm optimization with wavelet transform,” *IEEE Trans. Syst. Man, Cybern.*, vol. 44, no. 1, pp. 111–120, Jan. 2014.

- [20] D. Li, J. Weng, X. Chu, and J. Zhang, "A network deployment strategy for home area networks in smart grid," in *Proc. IEEE Int. Symp. Personal, Indoor and Mobile Radio Commun.*, Hong Kong, China, 2015, pp. 2160–2165.
- [21] W. Cui, Y. Zhang, L. Wei, and M. Lu, "Optimizing base stations deployment in wireless access networks for smart grids," in *Proc. Int. Conf. Wireless Commun. and Signal Process.*, Nanjing, China, 2015, pp. 1–5.
- [22] H. Liang, B. Wang, W. Liu, and H. Xu, "A novel transmitter placement scheme based on hierarchical simplex search for indoor wireless coverage optimization," *IEEE Trans. Antennas and Propag.*, vol. 60, no. 8, pp. 3921–3932, Aug. 2012.
- [23] I. Siomina, P. Varbrand, and D. Yuan, "Automated optimization of service coverage and base station antenna configuration in UMTS networks," *IEEE Wireless Commun.*, vol. 13, no. 6, pp. 16–25, Dec. 2006.
- [24] G. Tan, S. A. Jarvis, and A. M. Kermarrec, "Connectivity-guaranteed and obstacle-adaptive deployment schemes for mobile sensor networks," *IEEE Trans. Mobile Comput.*, vol. 8, no. 6, pp. 836–848, Jun. 2009.
- [25] G. Wang, G. Cao, and T. L. Porta, "Movement-assisted sensor deployment," *IEEE Trans. Mobile Comput.*, vol. 5, no. 6, pp. 640–652, Jun. 2006.
- [26] B. J. Farahani, H. Ghaffarian, and M. Fathy, "A fuzzy based priority approach in mobile sensor network coverage," *Int. J. Netw. Security*, vol. 2, no. 1, pp. 138–143, Nov. 2009.
- [27] X. Jiang, Y. P. Chen, and T. Yu, "Localized distributed sensor deployment via coevolutionary computation," in *Proc. Int. Conf. Commun. and Netw.*, Hangzhou, China, 2008, pp. 785–789.
- [28] C. S. Sahin, E. Urrea, M. Uyar, M. Conner, I. Hokelek, G. Bertoli, and C. Pizzo, "Self-deployment of mobile agents in manets for military applications," in *Proc. Conf. Army Sci.*, 2008.
- [29] D. B. Jourdan and O. L. D. Weck, "Layout optimization for a wireless sensor network using a multi-objective genetic algorithm," in *Proc. 59th IEEE Conf. Veh. Technol.*, vol. 5, no. 5, 2004, pp. 2466–2470.
- [30] K. Chakrabarty, S. S. Iyengar, H. Qi, and E. Cho, "Grid coverage for surveillance and target location in distributed sensor networks," *IEEE Trans. Comput.*, vol. 51, no. 12, pp. 1448–1453, Dec. 2002.
- [31] Q. Wu, R. S. V. Nageswara, D. Xiaojiang, S. S. Iyengar, and V. K. Vaishnavi, "On efficient deployment of sensors on planar grid," *Comput. Commun.*, vol. 30, no. 14, pp. 2721–2734, Oct. 2007.
- [32] H. Zhang, J. Wang, T. Lu, and T. A. Gulliver, "Capacity of 60 GHz wireless communication systems over Ricean fading channels," in *Proc. IEEE Pacific Rim Conf. Commun., Comput. and Signal Process.*, Victoria, BC, Canada, 2011, pp. 437–440.
- [33] Y. Li, Y. an Liu, and P. Luo, "Link probability based opportunistic routing metric in wireless network," in *Proc. Int. Conf. Commun. and Mobile Comput.*, Yunnan, China, 2009, pp. 308–312.
- [34] S. Zhou, M. Zhao, X. Xu, J. Wang, and Y. Yao, "Distributed wireless communication system: a new architecture for future public wireless access," *IEEE Commun. Mag.*, vol. 41, no. 3, pp. 108–113, Mar. 2003.
- [35] Y. Dong, W. K. Hon, D. K. Y. Yau, and J. C. Chin, "Distance reduction in mobile wireless communication: lower bound analysis and practical attainment," in *Proc. 15th Int. Symp. Modeling, Anal., and Simulation of Comput. and Telecommun. Syst.*, Istanbul, Turkey, 2009, pp. 276–287.
- [36] J. Tian, M. Gao, and S. Zhou, "Modeling for mobile communication fading channel based on regression support vector machine," in *Proc. Int. Conf. Netw. Security, Wireless Commun. and Trusted Comput.*, Wuhan, China, 2009, pp. 683–687.
- [37] X. Zhang and J. G. Andrews, "Downlink cellular network analysis with multi-slope path loss models," *IEEE Trans. Commun.*, vol. 63, no. 5, pp. 1881–1894, May 2015.
- [38] H. T. Friis, "A note on a simple transmission formula," in *Proc. IRE*, 1946, pp. 254–256.
- [39] J. M. Taylor, R. Thaine, T. KayLee, K. Dakoda, L. Cody, and P. Makenzie, "Dynamic link budget simulation for high altitude balloon data link experiment," in *Proc. 18th Symp. Commun. and Netw.*, Alexandria, VA, USA, 2015, pp. 32–36.
- [40] D. S. J. D. Couto, D. Aguayo, J. Bicket, and R. Morris, "A high-throughput path metric for multi-hop wireless routing," *Wireless Netw.*, vol. 11, no. 4, pp. 419–434, Jul 2003.
- [41] M. O. Kilavuz and M. Yuksel, "Path approximation for multi-hop wireless routing under application-based accuracy constraints," *Comput. Netw.*, vol. 56, no. 1, pp. 345–364, Jan. 2012.
- [42] S. M. Das, H. Pucha, K. Papagiannaki, and Y. C. Hu, "Studying wireless routing link metric dynamics," in *Proc. 7th ACM SIGCOMM Conf. Internet Meas.*, San Diego, CA, USA, 2007, pp. 327–332.
- [43] Q. Zhang and H. Li, "MOEA/D: A multiobjective evolutionary algorithm based on decomposition," *IEEE Trans. Evol. Comput.*, vol. 11, no. 6, pp. 712–731, Dec. 2007.
- [44] H. Li, M. Gong, Q. Wang, J. Liu, and L. Su, "A multiobjective fuzzy clustering method for change detection in SAR images," *Appl. Soft Comput.*, vol. 46, pp. 767–777, Sept. 2016.
- [45] M. Gong, M. Zhang, and Y. Yuan, "Unsupervised band selection based on evolutionary multiobjective optimization for hyperspectral images," *IEEE Trans. Geosci. Remote Sens.*, vol. 54, no. 1, pp. 544–557, Jan. 2016.
- [46] S. Wang, M. Gong, H. Li, and J. Yang, "Multi-objective optimization for long tail recommendation," *Knowl. Based Syst.*, vol. 104, pp. 145–155, Jul. 2016.
- [47] Q. Cai, M. Gong, S. Ruan, Q. Miao, and H. Du, "Network structural balance based on evolutionary multiobjective optimization: A two-step approach," *IEEE Trans. Evol. Comput.*, vol. 19, no. 6, pp. 903–916, Apr. 2015.
- [48] L. Li, X. Yao, R. Stolk, M. Gong, and S. He, "An evolutionary multiobjective approach to sparse reconstruction," *IEEE Trans. Evol. Comput.*, vol. 18, no. 6, pp. 827–845, Oct. 2014.
- [49] L. Wang, Q. Zhang, A. Zhou, M. Gong, and L. Jiao, "Constrained subproblems in decomposition based multiobjective evolutionary algorithm," *IEEE Trans. Evol. Comput.*, vol. 20, no. 3, pp. 475–480, Jun. 2016.
- [50] D. K. Saxena, A. Sinha, J. A. Duro, and Q. Zhang, "Entropy based termination criterion for multi-objective evolutionary algorithms," *IEEE Trans. Evol. Comput.*, vol. 20, no. 4, pp. 485–498, Aug. 2016.
- [51] X. Cai, Y. Li, Z. Fan, and Q. Zhang, "An external archive guided multiobjective evolutionary algorithm based on decomposition for combinatorial optimization," *IEEE Trans. Evol. Comput.*, vol. 19, no. 4, pp. 508–523, Aug. 2015.
- [52] K. Deb, A. Pratap, S. Agarwal, and T. Meyarivan, "A fast and elitist multiobjective genetic algorithm: NSGA-II," *IEEE Trans. Evol. Comp.*, vol. 6, no. 2, pp. 182–197, Apr. 2002.
- [53] I. Giagkiozis, R. C. Purshouse, and P. J. Fleming, *Generalized Decomposition*. Berlin Germany: Springer, 2013.
- [54] M. Gong, X. Jiang, and H. Li, "Optimization methods for regularization-based Ill-posed problems: a survey and a multi-objective framework," *Frontiers of Comput. Sci.*, pp. 1–30, 2016.
- [55] M. Gong, H. Li, and X. Jiang, "A multi-objective optimization framework for Ill-posed inverse problems in image processing," *CAAI Trans. Intell. Technol.*, vol. 1, no. 3, pp. 225–240, Jul. 2016.
- [56] J. Bader and E. Zitzler, "Hype: an algorithm for fast hypervolume-based many-objective optimization," *MIT Evol. Comput.*, vol. 19, no. 1, pp. 45–76, Mar. 2011.
- [57] L. Ma, M. Gong, J. Yan, and F. Yuan, "A decomposition-based multiobjective evolutionary algorithm for analyzing network structural balance," *Inf. Sci.*, vol. 378, pp. 144–160, 2017.
- [58] H. Li and Q. Zhang, "Multiobjective optimization problems with complicated pareto sets, MOEA/D and NSGA-II," *IEEE Trans. Evol. Comput.*, vol. 13, no. 2, pp. 284–302, Apr. 2009.
- [59] K. Deb, L. Zhu, and S. Kulkarni, "Multi-scenario, multi-objective optimization using evolutionary algorithms: Initial results," in *Proc. IEEE Congr. Evol. Comput.*, Sendai, Japan, 2015, pp. 1877–1884.
- [60] N. Chen, W. Chen, Y. Gong, Z. Zhan, J. Zhang, Y. Li, and Y. Tan, "An evolutionary algorithm with double-level archives for multiobjective optimization," *IEEE Trans. Cybern.*, vol. 45, no. 9, pp. 1851–1863, Sept. 2015.
- [61] H. Ishibuchi, Y. Tanigaki, H. Masuda, and Y. Nojima, *Distance-Based Analysis of Crossover Operators for Many-Objective Knapsack Problems*. Berlin Germany: Springer, 2014.



**Maoguo Gong** (M'07-SM'14) received the B.S. degree in electronic engineering (first class honors) and the Ph.D. degree in electronic science and technology from Xidian University, Xi'an, China, in 2003 and 2009, respectively.

Since 2006, he has been a Teacher with Xidian University. In 2008 and 2010, he was promoted as an Associate Professor and as a Full Professor, respectively, both with exceptive admission. His research interests are in the area of computational intelligence with applications to optimization, learning, data mining and image understanding.

Dr. Gong received the prestigious National Program for the support of Top-Notch Young Professionals from the Central Organization Department of China, the Excellent Young Scientist Foundation from the National Natural Science Foundation of China, and the New Century Excellent Talent in University from the Ministry of Education of China. He is the Vice Chair of the IEEE Computational Intelligence Society Task Force on Memetic Computing, an Executive Committee Member of the Chinese Association for Artificial Intelligence, and a Senior Member of the Chinese Computer Federation. Please see his homepage (<http://see.xidian.edu.cn/faculty/mggong>) for more information.



**Zhao Wang** received the B.S. degree in intelligence science and technology from Xidian University, Xi'an, China, in 2011, where he is currently pursuing the Ph.D. degree. His current research interests include computational intelligence and distributed computing.



**Zexuan Zhu** received the B.S. degree in computer science and technology from Fudan University, Shanghai, China, in 2003, and the Ph.D. degree in computer engineering from Nanyang Technological University, Singapore, in 2008. He is currently an Associate Professor with the College of Computer Science and Software Engineering, Shenzhen University, Shenzhen, China. His current research interests include computational intelligence, machine learning, and bioinformatics.



**Licheng Jiao** (SM'89) received the B.S. degree from Shanghai Jiao Tong University, Shanghai, China, in 1982 and the M.S. and Ph.D. degrees from Xian Jiaotong University, Xian, China, in 1984 and 1990, respectively.

Since 1992, he has been a Professor with the School of Electronic Engineering, Xidian University, Xian, where he is currently the Director of the Key Laboratory of Intelligent Perception and Image Understanding of the Ministry of Education of China, International Research Center of Intelligent Perception and Computation. His current research interests include intelligent information processing, image processing, machine learning, and pattern recognition. Prof. Jiao is a member of the IEEE Xian Section Execution Committee; the President of the Computational Intelligence Chapter, the IEEE Xian Section, and the IET Xian Network; the Chairman of the Awards and Recognition Committee; the Vice Board Chairperson of the Chinese Association of Artificial Intelligence; a Councilor of the Chinese Institute of Electronics; a Committee Member of the Chinese Committee of Neural Networks; and an Expert of the Academic Degrees Committee of the State Council.